Down-delta hydraulic geometry and its application to the rock record

O.A. Prasojo[1,2*], T. B. Hoey[3], A. Owen[1] and R.D. Williams[1]

[1]School of Geographical and Earth Sciences, University of Glasgow, Glasgow, G12 8QQ, United Kingdom, o.prasojo.1@research.gla.ac.uk, Amanda.Owen@glasgow.ac.uk, Richard.Williams@glasgow.ac.uk

[2]Geoscience Study Program, Faculty of Mathematics and Natural Sciences (FMIPA), Universitas Indonesia, Depok 16424, Indonesia

[3]Department of Civil and Environmental Engineering, Brunel University London, Uxbridge, UB8 3PH, United Kingdom, Trevor.Hoey@brunel.ac.uk

The following preprint is under review at **Sedimentology** by Prasojo, O. A., Hoey, T. B., Owen, A., & Williams, R. D.

ABSTRACT

Paleodischarge estimation is largely undertaken within fluvial settings, and there are limited paleodischarge estimates specifically from delta deposits, despite their significance globally. Making water paleodischarge estimates for deltas using catchment-based approaches developed using data from fluvial settings requires estimation of parameters from the rock record (e.g. paleotemperature, paleoslope, paleorelief) that may be difficult to determine, and may lead to under- or over-estimation of paleodischarge values due to differences in process-form relationships between alluvial rivers and deltas. When a sediment-conveying fluvial channel starts to debouch into a standing body of water, delta lobes develop through repeating mouth bar deposition due to flow deceleration, forming a deltaic morphology with distributary channel networks that differ morphologically from those developed in unidirectional flowing alluvial rivers. This study provides empirical relationships determined across five climate regions, using 3823 measurements of distributary channel width from 66 river deltas alongside their bankfull discharge, by applying the concept of hydraulic geometry. Empirical relationships are developed from the global delta dataset between bankfull discharge and catchment area (Q_b-A) and also bankfull discharge and distributary channel width (Q_b-W). These empirical relationships produce very strong statistical correlations, especially between Q_b and W, across different climate regions ($Q_b = 0.34W^{1.48}$, $R^2 = 0.77$). However, both Q_b-A and Q_b-W relationships have outliers that may be explained by particular hydrological or geomorphic conditions. These new empirical relationships derived from modern systems are applied to Cretaceous outcrops (Ferron Sandstone, Dunvegan and McMurray formations). The comparatively simple scaling relationships derived here produced paleodischarge estimates within the same orderc of magnitude as the paleodischarge values derived from existing, more complex approaches. Our study contributes to source-to-sink investigations by enabling

paleodischarge estimates that intrinsically account for climate impacts on channel geometry at the time of deposition, using measurements of channel width or catchment area of a deltaic outcrop.

1. INTRODUCTION

Fluvial paleodischarge estimates are often made using empirical scaling relationships (Milliman & Syvitski, 1992; Syvitski & Morehead, 1999; Syvitski, 2002; Syvitski *et al.*, 2003; Syvitski & Saito, 2007; Davidson & North, 2009; Holbrook & Wanas, 2014; Eide *et al.*, 2018; Brewer *et al.*, 2020). Results derived from these scaling relationships play important roles in reservoir volume assessment, inferences of climate and tectonic forcing, and comparative paleohydraulic estimates across various types of river systems in source-to-sink studies (Montgomery & Gran, 2001; Merritt & Wohl, 2003; Bhattacharya & Tye, 2004; Brardinoni & Hassan, 2006; Wohl & David, 2008; Davidson & Hartley, 2010; Eaton, 2013). Despite their abundance in the rock record, delta channels have infrequently been used to estimate paleodischarge (Mikhailov, 1970; Andrén, 1994; Edmonds & Slingerland, 2007; Sassi *et al.*, 2012; Gleason, 2015).

Delta channels have different flow conditions from the unidirectional flow of fluvial channels due to bidirectional flow in some parts of deltas and widespread influence of the backwater generated by the elevation of the receiving water body. The presence of a backwater decelerates and sometimes reverses the unidirectional flow of water influx from the alluvial rivers (Nittrouer, 2013; Gugliotta & Saito, 2019; Wu & Nittrouer, 2019). When a sediment-conveying fluvial channel starts to debouch into a standing body of water, delta lobes initially develop through mouth bar deposition due to backwater-generated flow deceleration. Multiple successive mouthbars accumulated in front of a river mouth form the characteristic distributary deltaic morphology with channel networks that merge upstream at the delta apex (Edmonds &

Slingerland, 2007). The split between two or more newly formed distributary channels occurs due to this mouth bar deposition (Wright, 1977; Edmonds & Slingerland, 2007; Kleinhans *et al.*, 2013). Hence, any estimate of flow discharge in a deltaic system will be incomplete if only a single distributary channel is considered. In addition, open water deltas are typically exposed to marine processes in the form of tides, wave energy, storm surges, lake level and sea-level change (Galloway, 1975; Wright, 1977; Hoitink *et al.*, 2017). Due to the presence of marine processes, the unidirectional fluvial channel flow becomes less prominent particularly closer to the shoreline (Hoitink *et al.*, 2017; Gugliotta *et al.*, 2019). In the proximal parts of deltas, channels are fluvially controlled and fluvial morphometric relationships apply; once the channel is influenced by marine processes, this scaling may change. In the distal part of a delta, the presence of large tidal, wave energy or backwater-controlled flow regimes will significantly alter the geometry of delta distributary channels both in modern systems and in the rock record (Chatanantavet *et al.*, 2012; Lamb *et al.*, 2012; Nittrouer, 2013; Rossi *et al.*, 2016; Fernandes *et al.*, 2016; Ganti *et al.*, 2016; Rossi & Steel, 2016; Martin *et al.*, 2018; Chadwick *et al.*, 2019, 2020; Gugliotta & Saito, 2019).

There is a need to understand morphometric scaling relationships in deltaic systems as these are likely to differ from fluvial systems because of the marine processes that directly influence delta distributary channel geometry. Here, we use globally-available satellite imagery, catchment area and river discharge datasets to build empirical scaling relationships between delta distributary channel widths, river catchment area and water discharge. The aims of this paper are thus to: (1) estimate the relationship between bankfull river discharge (Q_b) and catchment area (A) across different climates (Q_b-A relationship), for modern river deltas; (2) estimate the relationship between bankfull discharge and delta distributary channel widths (W) across different climates (Q_b-W relationship); and, (3) outline and discuss how these relationships may be employed in deep-time stratigraphic successions, particularly where proxies for paleoclimate can be retrieved. Such empirical relationships enable paleogeographic reconstruction using modern systems, particularly where based on geometric properties that can be easily extracted from geologic deposits. Empirical scaling relationships could aid our global understanding of delta hydraulic geometry, both for modern and ancient systems (Mikhailov, 1970; Andrén, 1994; Edmonds & Slingerland, 2007; Sassi *et al.*, 2012; Gleason, 2015).

2. PREVIOUS APPROACHES AND JUSTIFICATION OF THE NEW APPROACH

Paleodischarge can be estimated through several approaches including geometric scaling relationships (e.g. between channel width and discharge), hydraulic calculations (e.g. derived from grain size, and sedimentary structures, such as the Fulcrum model - Holbrook & Wanas (2014)), and multivariate statistical equations relating, for example, the catchment erodibility (B), water discharge (Q), area (A), relief (R) and annual temperature (T) (the 'BQART' model - Syvitski & Milliman (2007)). Some of these approaches require measurements or estimates of parameters that are commonly challenging to obtain from rock record datasets (e.g. paleotemperature, relief, paleoslope, catchment area, bankfull depth) (Syvitski & Saito, 2007; Davidson & North, 2009; Holbrook & Wanas, 2014; Brewer *et al.*, 2020). All available methods make assumptions, for example when using geometric scaling the channel geometry is assumed to be in equilibrium with the bankfull water discharge.

One of the most commonly used models, the Fulcrum model, assumes dynamic equilibrium where all sediment mass transported through a trunk channel is balanced by sediment mass eroded upstream and deposited downstream (Holbrook & Wanas, 2014). This model also assumes a fixed position and dimension of a rectangular paleochannel geometry. Values of dimensionless bankfull Shields' stress and the Chezy friction coefficient are assumed, from which paleoslope, velocity and bankfull depth hence paleodischarge are calculated (Brewer *et al.*, 2020; Lyster *et al.*, 2021). The Shield's stress (Ganti *et al.*, 2019) and median formative flow depth (Trampush *et al.*, 2014) are challenging to estimate from ancient deposits, although they can be constrained using information on, for example, grain-size distribution.

The second widely applied model for estimating paleodischarge is the 'BQART' model, which utilizes catchment-scale parameters. Although the original goal of this model was to estimate the total suspended solid load (TSS) brought by the fluvial system to the ocean, it can be used to estimate discharge or paleodischarge and is applicable to ancient sedimentary systems (e.g. Blum & Hattier-Womack, 2009; Sømme *et al.*, 2011; Allen *et al.*, 2013; Watkins *et al.*, 2019). The 'BQART' model parameters can often be only partially constrained. For example, estimating paleotemperature relies on proxy information (e.g. biomes of flora and fauna, paleosols, mineralogy) combined with plate tectonic reconstructions, which increase the uncertainty in 'BQART' sediment load estimates, especially in cooler climates (Nyberg *et al.*, 2021).

Scaling between discharge and channel width and depth is an inevitable consequence of channel size adjusting to the volume of water being conveyed. Hydraulic geometry provides a theoretical basis for such scaling. Hydraulic geometry refers to empirical relationships relating channel width (*W*), depth (*d*) and velocity (*v*) to discharge (*Q*) (Leopold & Maddock, 1953). As discharge fluctuates at a single site, strong power relationships of the following form are found:

$W = aQ^b$ (*W*-*Q* relationship) (1A)

$d = cQ^f$ (*d*-*Q* relationship) (1B)

$v = kQ^m$ (*v*-*Q* relationship) (1C)

with the coefficients (*a*, *c*, *k*) and exponents (*b*, *f*, *m*) derived empirically from repeat measurements (Leopold & Maddock, 1953). From the continuity equation *Q* = *W.d.v*, it follows that *a.c.k* =

(b+f+m) = 1. The values of b, f and m are constrained by the hydraulics of water flow (Ferguson, 1986). For a discharge of specified recurrence interval, such as bankfull discharge, consistent downstream hydraulic geometry relationships exist, taking the same form as Eq. 1. In distributary deltas, the downstream relationships reflect abrupt reductions in discharge at bifurcations and also the increasing influence of bidirectional flow towards the downstream margin of the delta. Hence, 'down-delta' hydraulic geometry is complex but at any location along a distributary channel Eq. 1 applies consistently due to the continuity of discharge.

Here, we investigate empirical relationships from 66 catchments feeding river deltas across different climate regions, that include 3823 distributary channel width measurements available at https://doi.org/10.6084/m9.figshare.19574938.v2 (Fig. 1A). We relate catchment areas and their associated bankfull discharges to the median channel width measured across each delta. The median is chosen for three reasons: firstly, it provides a more conservative estimate of central tendency than the mean in cases where there may be very wide channels close to the downstream limit of the delta; secondly, the preservation potential of delta channel deposits is greater away from the downstream limit and the median thus better represents channels that are likely to be preserved (Olariu & Bhattacharya, 2006); and, in ancient deposits the number of preserved channels will often be small and the influence of outliers is reduced by using the median. Assuming that the measured distributary channel widths are approximately bankfull widths, scaling relationships are determined between the measured median distributary channel widths and Q_2 (2-year recurrence flood as an estimate of bankfull discharge, Q_b) in the river, and between catchment area and Q_2 (Leopold & Maddock, 1953; Gleason, 2015). A re-arrangement of Eq. 1A, $Q_b = \alpha w^{\beta}$ (Q_b-W relationship) is used as this provides a basis for sedimentologists to estimate bankfull discharge from channel widths, measurement of which is often achievable in ancient deposits.

3. METHODS

Empirical statistical relationships were found between the median widths of delta distributary channels gathered from satellite imagery and their site-specific discharges. Although backwater effects in the form of wave and tidal influences may be present, other studies have demonstrated the effectiveness of this relationship in deltaic environments (Mikhailov, 1970; Andrén, 1994; Edmonds & Slingerland, 2007; Sassi *et al.*, 2012; Gleason, 2015). Bankfull discharge has widely been considered as the flow that controls channel geometry in alluvial rivers (De Rose *et al.*, 2008; Haucke & Clancy, 2011; Gleason, 2015), and is estimated here as Q_2, where 2 is the recurrence interval (years) of the discharge, as also used by others (Eaton, 2013, Jacobsen & Burr, 2016 and Morgan & Craddock, 2019).

Distributary channel widths on the 66 river deltas were measured in ArcGIS software using annual composite Landsat 5 satellite images. Delta apex (i.e. valley exit) locations were obtained from digital elevation models (DEM) from the Shuttle Radar Topography Mission (SRTM) and ArcticDEM (Tucker *et al.*, 2004; Farr *et al.*, 2007; Morin *et al.*, 2016) (Fig. 1A). Satellite imagery from 1984 were used where available, with some imagery dated to more recent years. Using the older (1984) images reduces the impact of infrastructure and bank protection on channel widths. The satellite images and DEMs were projected using World Geodetic System (WGS 1984) in ArcGIS to measure the channel widths and to extract valley exit locations (Hartley *et al.*, 2017).

River deltas were identified based on their protrusion beyond the original lateral shoreline (Caldwell *et al.*, 2019). Criteria for selecting river deltas includes any channel mouth that intersects with the open seawater, depositing sediment that protrudes beyond their lateral shoreline.

Nonetheless, we do not classify our river deltas based on their dominant forces (e.g. wave-, tide-, or river-dominated deltas) due to delta morphodynamics varying in time and space (e.g. a tide-dominated delta could transform into a river-dominated delta or a wave-dominated delta into a river-dominated delta) and very few delta end-members exist in nature (Syvitski & Saito, 2007). We also note that some influence of tide and wave processes may exist in the dataset (Correggiari et al., 2005; Ta et al., 2002). However, as this paper focuses on the estimation of river discharge from distributary channel morphology, we avoid river deltas with clear wave and tidal morphologies (e.g. abundant tidal creeks, deflected delta distributaries, elongated/parallel shoreline).

Channel widths were measured using a method, adapted from Sassi et al. (2012), in which a semicircular grid s/L is used to define a dimensionless distance from the delta apex to the shoreline, where s represents channelized distance from the delta apex and L is the channelized distance along the longest distributary channel (Fig. 1B). This grid allows measurement of the widths of multiple distributary channels located at the same dimensionless distance from the apex, hence allowing comparison across differently sized deltas. The apexes were defined as the valley exit points as recognized on DEMs (Hartley *et al.*, 2017) or as the most landward avulsion node within the delta (Ganti *et al.*, 2016). The semicircular grid has a resolution of ~10 times the width of the river channel at the first avulsion point to maintain consistent dimensionless distance and data frequency across deltas of varying size. As an example, the Mahakam delta, Indonesia, has a 500 m wide channel at the avulsion point which is ~40000 m following the longest channel from the shoreline (L). Channel widths are measured every 5000 m from the delta apex (i.e. $s/L = 0$) to the delta shoreline where $s/L = 1$ (Fig. 1C). Widths of distributary channels were included, and tidal creeks were omitted.

Catchment areas were delineated in ArcGIS using the watershed polygons available from the HydroBASINS dataset (Lehner & Grill, 2013). River discharge data for the closest measuring location to the delta apex were extracted from the Global Runoff Data Centre (GRDC) dataset (https://www.bafg.de/GRDC/EN/Home/homepage_node.html). The 2-year recurrence interval flood (Q_2) was used to estimate the bankfull discharge, or the dominant channel-forming flow, and is referred to as discharge (Q) subsequently for simplification (Wolman & Miller, 1960; Phillips & Jerolmack, 2016, 2019; Edwards *et al.*, 2019; Dunne & Jerolmack, 2020; Rhoads, 2020). Q_2 was calculated from daily discharge data using the Flow Analysis Summary Statistics Tool ('*fasstr*') package in R (https://github.com/bcgov/fasstr). For some locations, only monthly discharge data are available. Thus, conversion of Q_2 from monthly to daily was applied for each climate region (Beck *et al.*, 2018; Prasojo *et al.*, 2021). The climate region for each delta is defined based on a Köppen-Geiger climate classification map (Beck *et al.*, 2018).

The predictive Q-W_{med} relationships use the median channel width measured for each delta as statistically representative values of right-skewed channel width distributions (Fig. 2, 3). The 66 median width values were obtained from 3823 individual measurements (mean number of width measurements per delta = 58; range from 15 to 177) (Fig. 2). Note that these data do not allow prediction of the discharge/paleodischarge value of a single distributary channel, but enable calculation of the total riverine discharge that contributes sediment to builds the delta plain. Ordinary least square (OLS) regressions were then used to calculate power-law scaling relationships between both channel widths and catchment areas with bankfull discharge (Leopold & Maddock, 1953). We used OLS regression, which assumes error only in the dependent variable, as the aim is to produce predictive equations. The 95% confidence interval around the overall relationship for the 66 deltas is narrow, reflecting the statistical strength of the median channel width-bankfull discharge relationship across over three orders of magnitude of discharge. Using the regression equation to predict the discharge for an individual delta based on the estimate of the median channel width obtained from N width measurements yields a greater uncertainty (wider confidence interval) on account of the scatter in widths on individual deltas (blue shaded region in Fig. 2). The uncertainty in the median channel width estimate reduces as the number of width measurements increases since the uncertainty in the median decreases as a function of $N^{-1/2}$. OLS regressions were determined for each climate region to generate *Q*-*A* and *Q*-*W* morphometric scaling relationships.

The applicability of the power-law relationships determined from modern deltas was tested by applying the relationships to the channel widths and catchment areas derived from published outcrop data from Cretaceous formations in continental North America (Brownlie, 1983; Sageman & Arthur, 1994; Bhattacharya & MacEachern, 2009; Musial *et al.*, 2012; Bhattacharya *et al.*, 2016). Paleodischarges were estimated in these studies using the Fulcrum method applied to outcrop and subsurface data. These data were selected due to their relatively complete and observable exposures in the Ferron, Dunvegan and McMurray formations.

4. RESULTS

4.1. Data distribution

The 66 catchment areas are log-normally distributed (Fig. 3A), similar to the global fluvial system dataset (pink and blue lines on Fig. 3A) (Milliman & Farnsworth, 2011). The fluvial catchment areas (Milliman & Farnsworth, 2011) are not significantly different from the delta catchment areas used in this study ($t = 1.9$; $p < 0.06$).

The median width of delta channels is almost one order of magnitude larger than the median in the global river channel width database (Allen & Pavelsky, 2018; Fig. 3B, S1), although the range of widths are similar in both data sets. The channel widths in our delta data set are statistically significantly larger than in the fluvial data (t = -76.1; $p < 2.2\text{x}10^{-16}$). This difference suggests that scaling relationships from fluvial systems may not be able to be readily used for delta channels.

4.2. Water discharge and catchment area scaling relationship (*Q*-*A* relationship)

Globally, Fig. 4 shows a statistically significant (p = 3.3 x 10^{-8}; R^2 = 0.39; N = 66) power law relationship between catchment area and bankfull discharge, $Q_2 = 50.1A^{0.42}$ with 22 of the 66 deltas lying within the 95% confidence interval. Some of the more distant outliers are interpreted to be present due to extensive river engineering (e.g. embankments along riverbanks in Colorado, Nile and Ebro deltas) or due to wave and tide effects (e.g. Orinoco, Mackenzie, Godavari, Ob and Irrawaddy deltas). In comparison to the global river Q-A relationship ($Q = 0.075A^{0.8}$), the scaling relationship for global deltas has a non-significantly lower regression slope (p = 0.1) using the significance of the difference, or slope test (Syvitski & Milliman, 2007).

The relatively low R^2 value for the global data set can be explained in part by differences between climate regions. Separating the data into different climate regions produces significant relationships between A and Q_2 except in arid and cold regions where the relationships are not significant (R^2 = 0.24 and 0.25; p = 0.13 and 0.069; N = 11 and 14, respectively).

4.3. Water discharge and median channel width scaling relationship (*Q*-*W* relationship)

In total 66 paired measurements of discharge and median channel width were used to build the Q-W relationship. Overall, there is a statistically significant relationship with $Q_2 = 0.34W_{med}^{1.48}$ (R^2 = 0.77; p = 2.2 x 10^{-16}; N = 66) (Fig. 5). The Q-W relationship produces a better fit globally than the Q-A relationship above (Fig. 4A). In comparison to the global river Q-W relationship ($W = 17Q^{0.45}$) (Moody & Troutman, 2002), the Q-W delta channel relationship has a statistically significant lower regression slope ($p = 2.6\text{x}10^{-5}$). As an example, predicting the discharge from a delta with median channel width of 300 m will result in $Q_2 = 1576$ m^3/s, while the equivalent for a fluvial setting would be $Q_2 = 589$ m^3/s. Deltas have multiple channels, hence using $W_{med} = 300$ m will have maximum width of larger than 300 m near the apex (i.e. trunk channel), hence producing larger estimated bankfull discharge than the fluvial settings. These results suggest that predicting discharges from widths will produce different results if the channels are deltaic or fluvial.

When classified by climate region, *Q*-*W* relationships consistently show significant relationships ($p < 0.05$) with the strongest relationship for cold climates ($N = 14$) (Fig. 5A,C). Polar, temperate, and tropical regions also show strong relationships with R^2 values equal to 0.91, 0.88, 0.63, respectively (Fig. 5D-F). Similar to the *Q*-*A* relationship, the *Q*-*W* relationship from arid regions (N =11) shows the lowest R^2 although it is statistically significant ($p = 1.2 \times 10^{-2}$) (Fig. 5B).

In summary, compared with the *Q*-*A* relationships on Fig. 4A-F, the *Q*-*W* relationships proposed in this study consistently show more statistically significant ($p < 0.05$) relationships that also have higher R^2 values (Fig. 5A-F). The *Q*-*A* relationship from the temperate region is the strongest (Fig. 4E) and the strongest *Q*-*W* relationship is for the cold climate region (Fig. 5C). The weakest relationships consistently come from the arid settings from both *Q*-*A* and *Q*-*W* (Fig. 4B & 5B).

4.4. Application to the rock record

The scaling relationships obtained above from global modern river deltas are here applied to estimate paleodischarges from several deltaic deposits. Data were compiled from paleodischarge studies from well-exposed Cretaceous outcrops and subsurface dataset deposited in temperate-tropical climates. The data compiled from the literature used the Fulcrum approach to estimate paleodischarge values (Table 1).

The Ferron Sandstone, exposed near Ivie Creek, SW Utah, USA, is composed of Turonian (93.9-89.8 Ma) deltaic deposits from the western margin of the Western Interior Seaway (Bhattacharya & MacEachern, 2009; Braathen *et al.*, 2018) (Fig. 6). The delta prograded NE with an estimated drainage area of around 50000 km^2 (Bhattacharya & Tye, 2004). Previous paleodischarge studies on the Ferron Sandstone were based on trunk river characterization and estimation of paleoflow velocity from its grain size, bedform size and inferred flow depth. The interpretation of a tropical paleoclimate was obtained through facies analysis and catchment area is estimated from paleogeographic reconstructions.

The Cenomanian (100.5-93.9 Ma) Dunvegan Formation was deposited in a temperate climate, and contains deposits from a large delta complex that are predominantly massive and cross-bedded non-marine and marine sandstones (Plint, 2002). The delta complex prograded 400 km NW to SE into the actively subsiding foreland basin of Alberta. It is estimated that the delta had a catchment area of around 100000 km^2 (Bhattacharya & Walker, 1991; Sageman & Arthur, 1994; Bhattacharya & MacEachern, 2009; Plint, 2000; Hay & Plint, 2020).

The McMurray Formation (Barremian-Aptian; 130-112 Ma), NE Alberta, Canada, contains delta deposits in a N-NE direction in conjunction with the Rocky Mountains orogenesis (Musial *et al.*, 2012; Shinn *et al.*, 2014). The McMurray formation consists of wave rippled sands, highly burrowed sands, heterolithic sands and highly burrowed silts and muds deposited in a bay/deltaic setting (Musial *et al.*, 2012). Previous studies estimate the McMurray Formation had a paleodischarge of about 15000 m^3s^{-1} as the maximum bankfull discharge located at 56-58° North in temperate humid to mid-latitude warm humid climatic belt (Musial *et al.*, 2012; Martinius *et al.*, 2015).

Measured channel widths and estimated catchment areas were obtained from the literature that compiled subsurface dataset with outcrop observations (Sageman & Arthur, 1994; Plint & Wadsworth, 2003; Bhattacharya & MacEachern, 2009; Bhattacharya *et al.*, 2016) and were used to calculate paleodischarge using the equations calculated above from the modern systems. Four equations from our analysis of modern delta systems are used: (1) the global discharge-area relationship $Q_2 = 50.1A^{0.42}$ (Fig. 4A) (2) the climate-classified *Q*-*A* relationships, $Q_2 = 100A^{0.38}$ for the tropical region and $Q_2 = 15.9A^{0.54}$ for the temperate region (Fig. 4E,F); (3) the global discharge – width relationship (Fig. 5A) $Q_2 = 0.34W_{med}^{1.48}$; and (4) the climate-classified *Q*-*W* relationships, $Q_2 = W_{med}^{1.4}$ for the tropical region and $Q_2 = 0.07W_{med}^{1.66}$ for the temperate region (Fig. 5E,F). Paleodischarges were calculated using these equations and channel widths measured from the rock record obtained from previously published work. The paleodischarge values estimated using our equations were compared with previous paleodischarge estimates (Fig. 7) (Sageman & Arthur, 1994; Bhattacharya & MacEachern, 2009; Bhattacharya *et al.*, 2016).

Our new estimates of bankfull discharges lie within one order of magnitude of the paleodischarge values reported from the Fulcrum approach (Fig. 7) (Sageman & Arthur, 1994; Bhattacharya & MacEachern, 2009; Bhattacharya *et al.*, 2016). Note that the climate-classified *Q*-*W* relationship provides a better fit to the previous estimates than the global *Q*-*W* relationship. Conversely, the global *Q*-*A* relationship estimates correspond better to previous estimates than do estimates from scaling relationships for individual climate zones (Fig. 4E, F). Overall, the statistical models proposed in this study perform similarly to the established Fulcrum method by producing values within the same order of magnitude as the paleodischarge values derived from the literature.

5. DISCUSSION

5.1. Comparison to other paleodischarge estimations

Analysis of river discharges, catchment areas and median channel widths from 66 river deltas has generated new global equations $Q_2 = 50.1A^{0.42}$ and $Q_2 = 0.34W_{med}^{1.48}$. These relationships have also been classified by five climate regions (Table 2). Applying these comparatively simple equations to the rock record produced paleodischarge estimates within the same order of magnitude as the paleodischarge values derived from existing, more complex approaches.

The new relationships proposed in this study allow quantification of paleodischarge from the rock record based on measurements of channel width, estimates of paleoclimate and morphometric scaling relationships derived from modern systems. Our approach uses fewer input parameters to estimate paleodischarge than existing methods, the ‘BQART’ model or the Fulcrum model. Channel width is often measured from the rock record where channels are preserved, and cross-channel exposures are available. The proposed morphometric scaling relationships simplify paleohydrological calculations and enable more robust assessment of the uncertainties in the input parameter (channel width) to be accounted for when calculating paleodischarges.

In comparison to the Fulcrum and ‘BQART’ models that intrinsically include climate parameters, our work provides separate predictive equations for various climate regions. Our proposed models show statistically significant correlations, especially between channel width and bankfull discharge across different climate regions, that have not previously been explicitly accounted for (Table 2). These climate-classified models will benefit source-to-sink studies by providing calculations tailored to individual paleoclimates.

Nyberg *et al.* (2021) provide a comprehensive overview of the uncertainties, sensitivities and practicalities of the‘BQART’ model in estimating sediment load on geological timescales. They discussed in detail every parameter needed to estimate the paleodischarge and paleo-sediment load. For estimating the paleodischarge, the ‘BQART’ model uses a global *Q-A* power law scaling relationship similar to this study but without explicitly allowing for climate. Eide *et al.* (2018) added runoff (*Ro*) parameters to take into account the impact of climate by applying a different multiplier value to discharges calculated for each climate region (e.g. $Ro = 0.0005$ for arid and $Ro = 0.0161$ for humid regions). However, adding *Ro* constants shift the models, but does not change the models’ gradients. In contrast, we produce different equations for each climate region, allowing the models’ gradients to change, reflecting the role of soils or vegetation in controlling runoff. Also, the climate-classified models proposed in this study make paleodischarge estimation more straightforward if the paleoclimate can be deduced from the rock record.

Although the equations are statistically robust, defining paleoclimate from the rock record is not straightforward due to the often sparse exposure of preserved channels, complexities in stratigraphic correlation and the need for paleoclimate evidence. Reconstructing the relationship between evidence requires significant effort and may not always yield conclusive results (Shuman, 2014). Hence, it is reasonable to assess whether our climate—specific equations significantly improve paleodischarge estimates. ANOVA tests were used to compare the global *Q-W* and *Q-A* regression equations to the climate-classified *Q-W, Q-A* relationships. Comparing the global and the climate-classified *Q-W* regression lines produced $p= 0.62$. While the comparison of the global *Q-A* and climate-classified *Q-A* regression lines produced $p= 0.07$. Both of the tests showed that both global and climate-classified *Q-W* and *Q-A* relationships are not significantly different, hence could be used interchangeably. The tests imply that when the paleoclimate is challenging to be deduced from the rock record, the global *Q-W* or *Q-A* scaling relationship could be used instead.

5.2. Limitation of the proposed scaling relationships

For the *Q-A* and *Q-W* relationships, the standard error of residuals are 1.23 and 0.76 in log units, respectively. Despite overall significance of the regressions, additional factors may affect both relationships such as anthropogenic effects on channel width and/or river flows that may disrupt the dynamic equilibrium assumption that underpins the proposed scaling relationships (Aslan *et al.*, 2005; Li *et al.*, 2017; Ninfo *et al.*, 2018), vegetation type and density (Huang & Nanson, 1997), sediment load (Hey & Thorne, 1986), grain size (Eaton, 2013), anabranches of multi-thread channel systems (Tabata & Hickin, 2003), material forming the channel boundary (Ellis & Church, 2005) and flood variability for each climate region (Rodier & Roche, 1978). Although the accuracy of predictive models can be improved by adding more variables (Mosley, 1981) this addition leads to models becoming increasingly less applicable to the rock record. For example, using our calculations, paleodischarge can be determined from any data set in which a catchment area or channel width can be determined (e.g. outcrop or seismic). However, if other variables such as grain size or paleoslope are needed these additional data may not always be readily available. Thus, keeping the variables as simple as possible (e.g. catchment areas and channel widths) is beneficial in creating models that are applicable to the rock-record. Also, adding more variables does not necessarily result in an increase in model accuracy. Mosley (1981) showed that channel cross-sectional area (e.g. width, depth) is 90% controlled by the bankfull discharge, bed sediment size and bank sediment character, with only 30% of the variability being explained by morphologic variables (e.g. braiding and sinuosity index). For reconstruction purposes, there is merit in simplicity and careful examination of the contributing factors of channel cross section and bankfull discharge should be undertaken before adding in more variables into the morphometric scaling relationships proposed in this study.

The prediction intervals for palaeodischarge (Table 1; Fig. 2) are wide because of scatter in the observations and the small number of width measurements available for the prediction. These wide prediction intervals need to be acknowledged when using the proposed scaling relationships. Consequently, when applying the scaling relationships to the rock record they should be further constrained as far as possible using all contextual information gathered from the rock record (e.g. grain size, bedforms interpreted from sedimentary structures, stratigraphic position) to justify the paleodischarge estimation produced by this approach. Our source data set of modern measurements are spatially distributed across the delta in one time horizon, from which we determine a median width to use for prediction. However, deltas are depositional systems and due to transgression/regression measurements made in outcrop or from subsurface imaging may produce biased samples across the delta, hence yielding a biased estimate of median channel width, or may aggregate measurements across time horizons with different external controls, such as changing Q_2 due to climatic fluctuations. Hence, as noted above in the context of climate interpretation, applying the new statistical models to the rock record requires interpreting the stratigraphic context of the measured distributary channels. As more data become available, larger data sets, modern and ancient, will be able to be used to constrain what are ‘reasonable’ paleodischarge estimates. This constraint will be quantitative as more data sets such as those in Table 2, are obtained.

Our approach uses width measurements from satellite imagery as width is the most readily obtained measure of channel scale on such images. In outcrop or subsurface datasets it is commonly easier to measure distributary channel depths (*d*) than widths. Channel widths and depths are very highly correlated empirically and theoretically (Ferguson, 1986), and depth and width measurements from distributary channels reported in the literature are summarized in Table S1. Although the depth and width exponents in Eq. 1 are consistent, variations in the multipliers mean that the *W:d* ratio cannot be taken as a global constant due to the influence of additional factors on channel geometry (e.g. vegetation, bank sediment cohesion). Some studies have found that *W:d* varies with discharge (Wang & Li, 2011) or with the measurement location (Kästner *et al.*, 2017; Wang *et al.*, 2008).

To accommodate the complexity of the relationship between channel width and depth in river deltas, we assume that the flow was steady during the *W* and *d* measurements in Table S1, and in an equilibrium depth and slope. The range of measured *W:d* ratios is from 10-200 with typical values of *W:d* = 30:1 (e.g. Mississippi delta; (Nittrouer *et al.*, 2012) and Fly delta (Latrubesse, 2008)), to 100:1 (e.g. Yellow River delta (Wang *et al.*, 2008; Wang & Li, 2011), Amazon and Brahmaputra deltas (Latrubesse, 2008)) and the extreme value of *W:d* = 200:1 from Wax Lake and Lena deltas (Olariu & Bhattacharya, 2006) (Table S1). By assuming that delta channel *W:d* relationships globally lie within the range suggested by the available measurements, we rescale our *Q-W* relationship to yield a novel discharge-depth (*Q-d*) scaling for *W:d* = 30, 100 and 200 (Table S2). We then classify the *Q-d* scaling based on climate regions. All of the *Q-d* relationships are statistically significant, with different *W:d* ratios affecting scaling constants only.

5.3. Climate impacts on the proposed scaling relationships

Climate-classified *Q-W* relationships may produce more reliable paleodischarge results than either the *Q-A* relationships or the global *Q-W* relationship due to the direct impacts of climatic factors on channel geometry. Most of the climate-classified *Q-W* relationships have higher R^2 values (0.52-0.94) than the global *Q-W* relationship (R^2 = 0.77). The *Q-A* relationships have R^2

values of 0.39 for the global data, and 0.24-0.85 for the climate-classified relationships. This does not necessarily mean that *Q-A* relationships should not be used, but depending on the data availability from the rock record, both *Q-A* and *Q-W* relationships remain useful for inferring paleodischarge.

Climate-classified *Q-A* relationships should give more reliable predicted paleodischarges than a single global *Q-A* relationship due to discharge being directly controlled by rainfall and runoff in each climate region (McCabe & Wolock, 2016; Eide *et al.*, 2018). However, for paleodischarge studies catchment areas calculated from paleogeographic reconstructions may contain significant uncertainties due to the assumptions and interpretations involved in building paleogeographic maps. Hence, the ability to estimate paleodischarge through regional hydraulic geometry scaling relationships (Davidson & North, 2009) supported by provenance analysis (Blum *et al.*, 2017), remains constrained by scatter in the modern data and the need to supplement the calculations with further estimated variables. Errors of at least one order of magnitude are not uncommon (Bhattacharya *et al.*, 2016), but may provide valuable information that cannot be obtained by other means, or that supplements independent reconstructions of paleoenvironments.

Particular caution is required when estimating paleodischarge in arid and cold climates. Arid climates have annual rainfall between 150-200 mm (Thornthwaite, 1948) and a highly episodic runoff regime with flood flows lasting for only a few hours or days in a year (Rodier & Roche, 1978). This regime makes the definition of bankfull discharge challenging in this climate (Shamir *et al.*, 2012). As an example, it is common to have rapid intermittent high flood with low and steady flow period throughout the year in an arid region (e.g. due to snowmelt in Colorado river catchment and intermittently anabranching river during low flow) (Segura & Pitlick, 2010). Catchment area and bankfull duration are poorly correlated in arid regions (Dodov & Foufoula-

Georgiou, 2005), and interannual runoff irregularity and downstream loss of water are very significant in arid regions (Rodier & Roche, 1978).

In cold climate regions, flow may be non-continuous or substantially reduced in winter so reducing how representative Q_2 is as the bankfull discharge, also resulting in a weak correlation between catchment area and Q_2 (Beltaos & Prowse, 2009; Stonevičius *et al.*, 2014). Flood hydrology in this region depends on interactions between snow and ice cover, precipitation and air temperature, that may induce shifts in runoff over decadal timescales (Stewart *et al.*, 2005; Shiklomanov *et al.*, 2007). Consequently, bankfull discharge estimation from both modern and ancient systems in these two climate regions should consider hydrological conditions in the relevant climate zone.

5.4. Further developments

Although the relationships calculated herein produce realistic discharge estimates in Cretaceous deltas constrained by outcrop and subsurface data, there is a need to test these relationships across different aged systems across different climate belts to understand the extent to which they can be applied. Also, despite scaling relationships being available from modern estuaries (Diefenderfer *et al.*, 2008; Gisen & Savenije, 2015) and tide-influenced river deltas (Sassi *et al.*, 2012), development of similar rock-record focused scaling relationships for other systems (e.g. tidal creeks or other delta types) remains an area for further study.

Finally, our proposed method adopts metrics that are more easily extracted from the rock record and which is based on specific climate zones has potentially important implications with regards to assessment of hydrocarbon, hydrogen, geothermal and carbon capture and storage (CCS) sizes (Bhattacharya & Tye, 2004; Shinn *et al.*, 2014). In addition, it will help in deducing climate and tectonic forcing on systems and paleohydraulics across various types of depositional systems in source-to-sink studies (Montgomery & Gran, 2001; Merritt & Wohl, 2003; Brardinoni & Hassan, 2006; Wohl & David, 2008; Davidson & Hartley, 2010; Eaton, 2013).

6. CONCLUSION

We have obtained *Q-A* and $Q\text{-}W_{med}$ scaling relationships for 66 modern river deltas across different climate regions by extracting catchment areas for each delta, making 3823 distributary channel width measurements and calculating their associated bankfull discharges. These relationships are intended to provide quantitative information on source catchment properties from data typically available in the rock record. Applying the simple scaling relationships derived here from modern systems to the rock record, coupled with paleoclimate information, produced paleodischarge estimates within the same order of magnitude as paleodischarge values derived from existing, more complex, approaches that require a larger number of parameters. These new relationships promise enhanced deduction of climate and paleodischarges across various types of depositional systems in source-to-sink studies, assessment of hydrocarbon, hydrogen, geothermal and carbon capture and storage (CCS) sizes, and more accurate paleogeography interpretations. The relationships have been validated against data from some Cretaceous deltas, applying these scaling relationships to other paleoclimate regions, systems of different ages and to different types of deltaic environment, remain areas of further study.

ACKNOWLEDGMENTS

The authors thank Prof. Gary Hampson and other anonymous reviewers for constructive comments on earlier versions. This research was funded by an award from the Indonesia Endowment Fund for Education (LPDP) to Prasojo. The global river discharge dataset is available from The Global Runoff Data Centre (GRDC), 56068 Koblenz, Germany or and via the web (http://www.bafg.de/grdc.htm).

DATA AVAILABILITY STATEMENT

Data from this paper are publicly-available in https://doi.org/10.6084/m9.figshare.19574938.v2.

REFERENCES

Allen, P.A., **Armitage, J.J.**, **Carter, A.**, **Duller, R.A.**, **Michael, N.A.**, **Sinclair, H.D.**, **Whitchurch, A.L.** and **Whittaker, A.C.** (2013) The Qs problem: Sediment volumetric balance of proximal foreland basin systems. *Sedimentology*, **60**, 102–130.

Andrén, H. (1994) Development of the Laitaure Delta, Swedish Lappland. *Uppsala Universitet*, 188 pp.

Aslan, A., **Autin, W.J.** and **Blum, M.D.** (2005) Causes of river avulsion: Insights from the late Holocene avulsion history of the Mississippi River, U.S.A. *J. Sediment. Res.*, **75**, 650–664.

Beck, H.E., **Zimmermann, N.E.**, **McVicar, T.R.**, **Vergopolan, N.**, **Berg, A.** and **Wood, E.F.** (2018) Present and future köppen-geiger climate classification maps at 1-km resolution. *Sci. Data*, **5**, 1–12.

Beltaos, S. and **Prowse, T.** (2009) River-ice hydrology in a shrinking cryosphere. *Hydrol. Process.*, **23**, 122–144.

Bhattacharya, J. and **Walker, R.G.** (1991) Allostratigraphic subdivision of the Upper Cretaceous Dunvegan, Shaftesbury, and Kaskapau formations in the northwestern Alberta subsurface. *Bull. Can. Pet. Geol.*, **39**, 145–164.

Bhattacharya, J.P., **Copeland, P.**, **Lawton, T.F.** and **Holbrook, J.** (2016) Estimation of source area, river paleo-discharge, paleoslope, and sediment budgets of linked deep-time depositional systems and implications for hydrocarbon potential. Earth-Science Rev. 153:77–110.

Bhattacharya, J.P. and **MacEachern, J.A.** (2009) Hyperpycnal Rivers and Prodeltaic Shelves in the Cretaceous Seaway of North America. *J. Sediment. Res.*, **79**, 184–209.

Bhattacharya, J.P. and **Tye, R.S.** (2004) Searching for modern Ferron analogs and application to subsurface interpretation. In: *Regional to Wellbore Analog for Fluvial–Deltaic Reservoir Modeling: the Ferron Sandstone of Utah: American Association of Petroleum Geologists, Studies in Geology 50* (Ed. T.C. Chidsey, R.D. Adams, and T.H. Morris), *American Association of Petroleum Geologists*, 39–57.

Blum, M.D. and **Hattier-Womack, J.** (2009) Climate Change, Sea-Level Change, and Fluvial Sediment Supply to Deepwater Depositional Systems. In: *External Controls of Deep-Water Depositional Systems* (Ed. B. Kneller, O.J. Martinsen, and B. McCaffrey), *SEPM (Society for Sedimentary Geology)*, 15–39.

Blum, M.D., **Milliken, K.T.**, **Pecha, M.A.**, **Snedden, J.W.**, **Frederick, B.C.** and **Galloway, W.E.** (2017) Detrital-zircon records of Cenomanian, Paleocene, and Oligocene Gulf of Mexico drainage integration and sediment routing: Implications for scales of basin-floor fans. *Geosphere*, **13**, 2169–2205.

Braathen, A., **Midtkandal, I.**, **Mulrooney, M.J.**, **Appleyard, T.R.**, **Haile, B.G.** and **van Yperen, A.E.** (2018) Growth-faults from delta collapse – structural and sedimentological investigation of the Last Chance delta, Ferron Sandstone, Utah. *Basin Res.*, **30**, 688–707.

Brardinoni, F. and **Hassan, M.A.** (2006) Glacial erosion, evolution of river long profiles, and the organization of process domains in mountain drainage basins of coastal British Columbia. *J. Geophys. Res.*, **111**, F01013.

Brewer, C.J., **Hampson, G.J.**, **Whittaker, A.C.**, **Roberts, G.G.** and **Watkins, S.E.** (2020) Comparison of methods to estimate sediment flux in ancient sediment routing systems. Earth-

Science Rev. 207:103217.

Brownlie, W.R. (1983) Flow Depth in Sand-Bed Channels. *J. Hydraul. Eng.*, **109**, 959–990.

Caldwell, R.L., **Edmonds, D.A.**, **Baumgardner, S.**, **Paola, C.**, **Roy, S.** and **Nienhuis, J.H.** (2019) A global delta dataset and the environmental variables that predict delta formation on marine coastlines. *Earth Surf. Dyn.*, **7**, 773–787.

Chadwick, A.J., **Lamb, M.P.** and **Ganti, V.** (2020) Accelerated river avulsion frequency on lowland deltas due to sea-level rise. *Proc. Natl. Acad. Sci. U. S. A.*, **117**, 17584–17590.

Chadwick, A.J., **Lamb, M.P.**, **Moodie, A.J.**, **Parker, G.** and **Nittrouer, J.A.** (2019) Origin of a Preferential Avulsion Node on Lowland River Deltas. *Geophys. Res. Lett.*, **46**, 4267–4277.

Chatanantavet, P., **Lamb, M.P.** and **Nittrouer, J.A.** (2012) Backwater controls of avulsion location on deltas. *Geophys. Res. Lett.*, **39**, 2–7.

Correggiari, A., **Cattaneo, A.** and **Trincardi, F.** (2005) Depositional Patterns in The Late Holocene Po Delta System. In: *SEPM Special Publication* (Ed. L. Giosan and J.P. Bhattacharya), *SEPM (Society for Sedimentary Geology)*, 365–392.

Davidson, S.K. and **Hartley, A.J.** (2010) Towards a quantitative method for estimating paleohydrology from clast size and comparison with modern rivers. *J. Sediment. Res.*, **80**, 688–702.

Davidson, S.K. and **North, C.P.** (2009) Geomorphological regional curves for prediction of drainage area and screening modern analogues for rivers in the rock record. *J. Sediment. Res.*, **79**, 773–792.

De Rose, R.C., **Stewardson, M.J.** and **Harman, C.** (2008) Downstream hydraulic geometry of rivers in Victoria, Australia. *Geomorphology*, **99**, 302–316.

Diefenderfer, H.L., **Coleman, A.M.**, **Borde, A.B.** and **Sinks, I.A.** (2008) Hydraulic geometry and microtopography of tidal freshwater forested wetlands and implications for restoration, Columbia River, U.S.A. *Ecohydrol. Hydrobiol.*, **8**, 339–361.

Dodov, B. and **Foufoula-Georgiou, E.** (2005) Fluvial processes and streamflow variability: Interplay in the scale-frequency continuum and implications for scaling. *Water Resour. Res.*, **41**, 1–18.

Dunne, K.B.J. and **Jerolmack, D.J.** (2020) What sets river width? *Sci. Adv.*, **6**, eabc1505.

Eaton, B.C. (2013) Hydraulic Geometry: Empirical Investigations and Theoretical Approaches. In: *Treatise on Geomorphology*, *Elsevier Inc.*, 9, 313–329.

Edmonds, D.A. and **Slingerland, R.L.** (2007) Mechanics of river mouth bar formation: Implications for the morphodynamics of delta distributary networks. J Geophys Res Earth Surf. doi: 10.1029/2006JF000574

Edwards, P.J., **Watson, E.A.** and **Wood, F.** (2019) Toward a Better Understanding of Recurrence Intervals, Bankfull, and Their Importance. *J. Contemp. Water Res. Educ.*, **166**, 35–45.

Eide, C.H., **Müller, R.** and **Helland-Hansen, W.** (2018) Using climate to relate water discharge and area in modern and ancient catchments. *Sedimentology*, **65**, 1378–1389.

Ellis, E.R. and **Church, M.** (2005) Hydraulic geometry of secondary channels of lower Fraser River, British Columbia, from acoustic Doppler profiling. *Water Resour. Res.*, **41**, 1–15.

Farr, T.G., **Rosen, P.A.**, **Caro, E.**, **Crippen, R.**, **Duren, R.**, **Hensley, S.**, **Kobrick, M.**, **Paller, M.**, **Rodriguez, E.**, **Roth, L.**, **Seal, D.**, **Shaffer, S.**, **Shimada, J.**, **Umland, J.**, **Werner, M.**, **Oskin, M.**, **Burbank, D.** and **Alsdorf, D.E.** (2007) The shuttle radar topography mission. Rev Geophys. doi: 10.1029/2005RG000183

Ferguson, R.I. (1986) Hydraulics and hydraulic geometry. *Prog. Phys. Geogr. Earth Environ.*, **10**, 1–31.

Fernandes, A.M., **Törnqvist, T.E.**, **Straub, K.M.** and **Mohrig, D.** (2016) Connecting the backwater hydraulics of coastal rivers to fluviodeltaic sedimentology and stratigraphy. *Geology*, **44**, 979–982.

Galloway, W.D. (1975) Process Framework for describing the morphologic and stratigraphic evolution of deltaic depositional systems. *Houst. Geol. Soc. Deltas Model. Explor.*, 87–98.

Ganti, V., **Chadwick, A.J.**, **Hassenruck-Gudipati, H.J.**, **Fuller, B.M.** and **Lamb, M.P.** (2016) Experimental river delta size set by multiple floods and backwater hydrodynamics. *Sci. Adv.*, **2**, e1501768.

Ganti, V., **Whittaker, A.C.**, **Lamb, M.P.** and **Fischer, W.W.** (2019) Low-gradient, single-threaded rivers prior to greening of the continents. *Proc. Natl. Acad. Sci.*, **116**, 11652–11657.

Gisen, J.I.A. and **Savenije, H.H.G.** (2015) Estimating bankfull discharge and depth in ungauged estuaries. *Water Resour. Res.*, **51**, 2298–2316.

Gleason, C.J. (2015) Hydraulic geometry of natural rivers: A review and future directions. *Prog. Phys. Geogr.*, **39**, 337–360.

Gugliotta, M. and **Saito, Y.** (2019) Matching trends in channel width, sinuosity, and depth along the fluvial to marine transition zone of tide-dominated river deltas: The need for a revision of depositional and hydraulic models. *Earth-Science Rev.*, **191**, 93–113.

Gugliotta, M., **Saito, Y.**, **Nguyen, V.L.**, **Ta, T.K.O.** and **Tamura, T.** (2019) Sediment distribution and depositional processes along the fluvial to marine transition zone of the Mekong River delta, Vietnam. *Sedimentology*, **66**, 146–164.

Hartley, A.J., **Weissmann, G.S.** and **Scuderi, L.** (2017) Controls on the apex location of large deltas. *J. Geol. Soc. London.*, **174**, 10–13.

Haucke, J. and **Clancy, K.A.** (2011) Stationarity of streamflow records and their influence on bankfull regional curves. *J. Am. Water Resour. Assoc.*, **47**, 1338–1347.

Hay, M.J. and **Plint, A.G.** (2020) High-frequency sequences within a retrogradational deltaic succession: Upper Cenomanian Dunvegan Formation, Western Canada Foreland Basin. *Depos. Rec.*, **6**, 524–551.

Hey, R.D. and **Thorne, C.R.** (1986) Stable Channels with Mobile Gravel Beds. *J. Hydraul. Eng.*, **112**, 671–689.

Hoitink, A.J.F., **Wang, Z.B.**, **Vermeulen, B.**, **Huismans, Y.** and **Kästner, K.** (2017) Tidal controls on river delta morphology. Nat. Geosci. 10:637–645.

Holbrook, J. and **Wanas, H.** (2014) A fulcrum approach to assessing source-to-sink mass balance using channel paleohydrologic paramaters derivable from common fluvial data sets with an example from the cretaceous of Egypt. *J. Sediment. Res.*, **84**, 349–372.

Huang, H.Q. and **Nanson, G.C.** (1997) Vegetation and channel variation; a case study of four small streams in southeastern Australia. *Geomorphology*, **18**, 237–249.

Jacobsen, R.E. and **Burr, D.M.** (2016) Greater contrast in Martian hydrological history from more accurate estimates of paleodischarge. *Geophys. Res. Lett.*, **43**, 8903–8911.

Kästner, K., **Hoitink, A.J.F.**, **Vermeulen, B.**, **Geertsema, T.J.** and **Ningsih, N.S.** (2017) Distributary channels in the fluvial to tidal transition zone. *J. Geophys. Res. Earth Surf.*, **122**, 696–710.

Kleinhans, M.G., **Ferguson, R.I.**, **Lane, S.N.** and **Hardy, R.J.** (2013) Splitting rivers at their seams: bifurcations and avulsion. *Earth Surf. Process. Landforms*, **38**, 47–61.

Lamb, M.P., **Nittrouer, J.A.**, **Mohrig, D.** and **Shaw, J.** (2012) Backwater and river plume controls on scour upstream of river mouths: Implications for fluvio-deltaic morphodynamics. *J. Geophys. Res*, **117**, 1002.

Latrubesse, E.M. (2008) Patterns of anabranching channels: The ultimate end-member adjustment of mega rivers. *Geomorphology*, **101**, 130–145.

Lehner, B. and **Grill, G.** (2013) Global river hydrography and network routing: Baseline data and new approaches to study the world's large river systems. *Hydrol. Process.*, **27**, 2171–2186.

Leopold, L.B. and **Maddock, T.** (1953) The Hydraulic Geometry of Stream Channels and Some Physiographic Implications. 57 pp.

Li, X., **Liu, J.P.**, **Saito, Y.** and **Nguyen, V.L.** (2017) Recent evolution of the Mekong Delta and the impacts of dams. *Earth-Science Rev.*, **175**, 1–17.

Lyster, S.J., **Whittaker, A.C.**, **Hampson, G.J.**, **Hajek, E.A.**, **Allison, P.A.** and **Lathrop, B.A.** (2021) Reconstructing the morphologies and hydrodynamics of ancient rivers from source to sink: Cretaceous Western Interior Basin, Utah, USA. Sedimentology. doi: 10.1111/sed.12877

Martin, J., **Fernandes, A.M.**, **Pickering, J.**, **Howes, N.**, **Mann, S.** and **McNeil, K.** (2018) The Stratigraphically Preserved Signature of Persistent Backwater Dynamics in a Large Paleodelta System: The Mungaroo Formation, North West Shelf, Australia. *J. Sediment. Res.*, **88**, 850–872.

Martinius, A.W., **Jablonski, B.V.J.**, **Fustic, M.**, **Strobl, R.** and **Van den Berg, J.H.** (2015) Fluvial to tidal transition zone facies in the McMurray Formation (Christina River, Alberta, Canada), with emphasis on the reflection of flow intensity in bottomset architecture. *Dev. Sedimentol.*, **68**, 445–480.

McCabe, G.J. and **Wolock, D.M.** (2016) Variability and Trends in Runoff Efficiency in the Conterminous United States. *JAWRA J. Am. Water Resour. Assoc.*, **52**, 1046–1055.

Merritt, D.M. and **Wohl, E.E.** (2003) Downstream hydraulic geometry and channel adjustment during a flood along an ephemeral, arid-region drainage. *Geomorphology*, **52**, 165–180.

Mikhailov, V.N. (1970) Hydrologic-morphometric characteristics of delta branches. *Stud. Rep. Hydrol.*, 146–158.

Milliman, J.D. and **Farnsworth, K.L.** (2011) River discharge to the coastal ocean: A global synthesis. *Cambridge University Press*, 1–384 pp.

Milliman, J.D. and **Syvitski, J.P.M.** (1992) Geomorphic/tectonic control of sediment discharge to the ocean: the importance of small mountainous rivers. *J. Geol.*, **100**, 525–544.

Montgomery, D.R. and **Gran, K.B.** (2001) Downstream variations in the width of bedrock channels. *Water Resour. Res.*, **37**, 1841–1846.

Moody, J.A. and **Troutman, B.M.** (2002) Characterization of the spatial variability of channel morphology. *Earth Surf. Process. Landforms*, **27**, 1251–1266.

Morgan, A.M. and **Craddock, R.A.** (2019) Assessing the Accuracy of Paleodischarge Estimates for Rivers on Mars. *Geophys. Res. Lett.*, **46**, 11738–11746.

Morin, P., **Porter, C.**, **Cloutier, M.**, **Howat, I.**, **Noh, M.-J.**, **Willis, M.**, **Bates, B.**, **Willamson, C.** and **Peterman, K.** (2016) ArcticDEM; A Publically Available, High Resolution Elevation Model of the Arctic. In: *Geophysical Research Abstracts*, *European Geosciences Union*, 18, 2016–8396.

Mosley, M.P. (1981) Semi-determinate hydraulic geometry of river channels, South Island, New Zealand. *Earth Surf. Process. Landforms*, **6**, 127–137.

Musial, G., **Reynaud, J.Y.**, **Gingras, M.K.**, **Féniès, H.**, **Labourdette, R.** and **Parize, O.** (2012) Subsurface and outcrop characterization of large tidally influenced point bars of the Cretaceous McMurray Formation (Alberta, Canada). *Sediment. Geol.*, **279**, 156–172.

Ninfo, A., **Ciavola, P.** and **Billi, P.** (2018) The Po Delta is restarting progradation: Geomorphological evolution based on a 47-years Earth Observation dataset. Sci Rep. doi:

10.1038/s41598-018-21928-3

Nittrouer, J.A. (2013) Backwater hydrodynamics and sediment transport in the lowermost Mississippi River delta: Implications for the development of fluvial-deltaic landforms in a large lowland river. In: *Proceedings of HP1, IAHS-IAPSO-IASPEI Assembly, Gothenburg, Sweden, July 2013 (IAHS Publ. 358, 2013).* (Ed. IAHS), *IAHS Publication*, Gothenburg, 358,

Nittrouer, J.A., **Shaw, J.**, **Lamb, M.P.** and **Mohrig, D.** (2012) Spatial and temporal trends for water-flow velocity and bed-material sediment transport in the lower Mississippi River. *Bull. Geol. Soc. Am.*, **124**, 400–414.

Nyberg, B., **Helland-Hansen, W.**, **Gawthorpe, R.**, **Tillmans, F.** and **Sandbakken, P.** (2021) Assessing First-Order BQART Estimates for Ancient Source-to-Sink Mass Budget Calculations. *Basin Res.*, **00**, 1–18.

Olariu, C. and **Bhattacharya, J.P.** (2006) Terminal distributary channels and delta front architecture of river-dominated delta systems. *J. Sediment. Res.*, **76**, 212–233.

Phillips, C.B. and **Jerolmack, D.J.** (2019) Bankfull Transport Capacity and the Threshold of Motion in Coarse-Grained Rivers. *Water Resour. Res.*, **55**, 11316–11330.

Phillips, C.B. and **Jerolmack, D.J.** (2016) Self-organization of river channels as a critical filter on climate signals. *Science (80-.).*, **352**, 694–697.

Plint, A.G. (2002) Paleovalley systems in the Upper Cretaceous Dunvegan Formation, Alberta and British Columbia. *Bull. Can. Pet. Geol.*, **50**, 277–296.

Plint, A.G. (2000) Sequence stratigraphy and paleogeography of a Cenomanian deltaic complex: the Dunvegan and lower Kaskapau formations in subsurface and outcrop, Alberta and British Columbia, Canada. *Bull. Can. Pet. Geol.*, **48**, 43–79.

Plint, A.G. and **Wadsworth, J.A.** (2003) Sedimentology and palaeogeomorphology of four large valley systems incising delta plains, western Canada Foreland Basin: implications for mid-Cretaceous sea-level changes. *Sedimentology*, **50**, 1147–1186.

Prasojo, O.A., **Hoey, T.B.**, **Owen, A.** and **Williams, R.D.** (2021) Slope break and avulsion locations scale consistently in global deltas. *Geophys. Res. Lett.*, e2021GL093656.

Rhoads, B.L. (2020) River Dynamics. *Cambridge University Press*.

Rodier, J. and **Roche, M.** (1978) River Flow in Arid Regions. In: *Hydrometry : principles and practices* (Ed. R. Herschy), *Wiley Blackwell*, 453–472.

Rossi, V.M., **Kim, W.**, **López, J.L.**, **Edmonds, D.**, **Geleynse, N.**, **Olariu, C.**, **Steel, R.J.**, **Hiatt, M.** and **Passalacqua, P.** (2016) Impact of tidal currents on delta-channel deepening, stratigraphic architecture, and sediment bypass beyond the shoreline. *Geology*, **44**, 927–930.

Rossi, V.M. and **Steel, R.J.** (2016) The role of tidal, wave and river currents in the evolution of mixed-energy deltas: Example from the Lajas Formation (Argentina). *Sedimentology*, **63**, 824–864.

Sageman, B.B. and **Arthur, M.A.** (1994) Early Turonian Paleogeographic/Paleobathymetric Map, Western Interior, U.S. In: *Mesozoic Systems of the Rocky Mountain Region, USA* (Ed. M. V. Caputo, J.A. Peterson, and K.J. Franczyk), *SEPM (Society for Sedimentary Geology)*, 457–470.

Sassi, M.G., **Hoitink, A.J.F.**, **de Brye, B.** and **Deleersnijder, E.** (2012) Downstream hydraulic geometry of a tidally influenced river delta. *J. Geophys. Res. Earth Surf.*, **117**, n/a-n/a.

Segura, C. and **Pitlick, J.** (2010) Scaling frequency of channel-forming flows in snowmelt-dominated streams. Water Resour Res. doi: 10.1029/2009WR008336

Shamir, E., **Ben-Moshe, L.**, **Ronen, A.**, **Grodek, T.**, **Enzel, Y.**, **Georgakakos, K.** and **Morin, E.** (2012) Hydrology and Earth System Sciences Discussions Geomorphology-based index for detecting minimal flood stages in arid alluvial streams. *Hydrol. Earth Syst. Sci. Discuss*, **9**, 12357–12394.

Shiklomanov, A.I., **Lammers, R.B.**, **Rawlins, M.A.**, **Smith, L.C.** and **Pavelsky, T.M.** (2007) Temporal and spatial variations in maximum river discharge from a new Russian data set. *J. Geophys. Res. Biogeosciences*, **112**, 4–53.

Shinn, Y.J., **Lee, H.S.**, **Kwon, Y.K.** and **Kwak, W.J.** (2014) Lithofacies distribution and depositional environment in the Lower Cretaceous McMurray Formation, BlackGold Lease, northern Alberta: implications for geometry and distribution of oil sand reservoirs. *Geosci. J.*, **18**, 325–337.

Shuman, B.N. (2014) Approaches to Paleoclimate Reconstruction. Ref Modul Earth Syst Environ Sci. doi: 10.1016/B978-0-12-409548-9.09405-7

Sømme, T.O., **Piper, D.J.W.**, **Deptuck, M.E.** and **Helland-Hansen, W.** (2011) Linking Onshore–Offshore Sediment Dispersal in the Golo Source-to-Sink System (Corsica, France) During the Late Quaternary. *J. Sediment. Res.*, **81**, 118–137.

Stewart, I.T., **Cayan, D.R.** and **Dettinger, M.D.** (2005) Changes toward Earlier Streamflow Timing across Western North America. *J. Clim.*, **18**, 1136–1155.

Stonevičius, E., **Valiuškevičius, G.**, **Rimkus, E.** and **Kažys, J.** (2014) Climate induced changes of Lithuanian rivers runoff in 1960–2009. *Water Resour. 2014 415*, **41**, 592–603.

Syvitski, J.P. and **Morehead, M.D.** (1999) Estimating river-sediment discharge to the ocean: application to the Eel margin, northern California. *Mar. Geol.*, **154**, 13–28.

Syvitski, J.P.M. (2002) Sediment discharge variability in Arctic rivers: implications for a warmer future. *Polar Res.*, **21**, 323–330.

Syvitski, J.P.M. and **Milliman, J.D.** (2007) Geology, Geography, and Humans Battle for

Dominance over the Delivery of Fluvial Sediment to the Coastal Ocean. *J. Geol.*, **115**, 1–19.

Syvitski, J.P.M., **Peckham, S.D.**, **Hilberman, R.** and **Mulder, T.** (2003) Predicting the terrestrial flux of sediment to the global ocean: a planetary perspective. *Sediment. Geol.*, **162**, 5–24.

Syvitski, J.P.M. and **Saito, Y.** (2007) Morphodynamics of deltas under the influence of humans. *Glob. Planet. Change*, **57**, 261–282.

Ta, T.K.O., **Nguyen, V.L.**, **Tateishi, M.**, **Kobayashi, I.**, **Saito, Y.** and **Nakamura, T.** (2002) Sediment facies and Late Holocene progradation of the Mekong River Delta in Bentre Province, southern Vietnam: An example of evolution from a tide-dominated to a tide- and wave-dominated delta. *Sediment. Geol.*, **152**, 313–325.

Tabata, K.K. and **Hickin, E.J.** (2003) Interchannel hydraulic geometry and hydraulic efficiency of the anastomosing Columbia River, southeastern British Columbia, Canada. *Earth Surf. Process. Landforms*, **28**, 837–852.

Thornthwaite, C.W. (1948) An Approach toward a Rational Classification of Climate. *Geogr. Rev.*, **38**, 55–94.

Trampush, S.M., **Huzurbazar, S.** and **McElroy, B.** (2014) Empirical assessment of theory for bankfull characteristics of alluvial channels. *Water Resour. Res.*, **50**, 9211–9220.

Tucker, C.J., **Grant, D.M.** and **Dykstra, J.D.** (2004) NASA's global orthorectified landsat data set. *Photogramm. Eng. Remote Sensing*, **70**, 313–322.

Wang, S. and **Li, Y.** (2011) Channel variations of the different channel pattern reaches in the lower Yellow River from 1950 to 1999. *Quat. Int.*, **244**, 238–247.

Wang, Z., **Wang, Z.** and **de Vriend, H.J.** (2008) Impact of water diversion on the morphological development of the Lower Yellow River. *Int. J. Sediment Res.*, **23**, 13–27.

Watkins, S.E., **Whittaker, A.C.**, **Bell, R.E.**, **McNeill, L.C.**, **Gawthorpe, R.L.**, **Brooke, S.A.S.**

and **Nixon, C.W.** (2019) Are landscapes buffered to high-frequency climate change? A comparison of sediment fluxes and depositional volumes in the Corinth Rift, central Greece, over the past 130 k.y. *GSA Bull.*, **131**, 372–388.

Wohl, E. and **David, G.C.L.** (2008) Consistency of scaling relations among bedrock and alluvial channels. *J. Geophys. Res.*, **113**, F04013.

Wolman, M.G. and **Miller, J.P.** (1960) Magnitude and Frequency of Forces in Geomorphic Processes. *J. Geol.*, **68**, 54–74.

Wright, L.D. (1977) Sediment transport and deposition at river mouths: A synthesis. *Bull. Geol. Soc. Am.*, **88**, 857–868.

Wu, C. and **Nittrouer, J.** (2019) Impacts of backwater hydrodynamics on fluvial-deltaic stratigraphy. *Basin Res.*, 1–18.

FIGURE CAPTIONS

Figure 1: (A) Distribution of the observed river deltas; (B,C) circular grid used to measure the channel widths from Mahakam delta, Indonesia (0°34'58.9"S, 117°16'39.7"E). Measured channel widths are red lines shown across wetted distributary channels. The spacing of the circular grid is ~10 times the channel width at the upstream limit of the delta. Stitched Landsat 5 images were taken from January 1994 via Google Earth Engine (GEE).

Figure 2: Illustration of the use of median distributary channel widths to obtain the predictive relationships between median distributary channel widths and bankfull discharge from 66 river deltas measured in this study. The green arrow on the y-axis shows the uncertainty on the discharge estimation, while the green arrow on the x-axis shows the uncertainty on the width measurement.

Figure 3: Catchment area and channel width distributions from this study, compared with data from Milliman and Farnsworth (2011) and Allen and Pavelsky (2018). (A) Distributions of catchment areas; (B) channel widths measured in this study; (C) boxplots of catchment areas measured in this study and by Milliman & Farnsworth (2011); (D) boxplots of channel widths measured in this study and by Allen & Pavelsky (2018). In (A) and (B), N is the sample number, S_{sk} is skewness, and t and p are the t-statistic and the associated probability from t-test comparison between the delta and fluvial datasets. The skewness values on (A) and (B) were calculated from the raw data, hence do not look skewed on log scales.

Figure 4: (A) Climate-classified bankfull discharge – catchment area (Q-A) relationship from all deltas; (B-F) Q-A relationships from the arid, cold, polar, temperate and tropical climate regions, respectively. Red continuous lines are Ordinary Least Squares (OLS) regressions for the data on each plot. The red dashed line on (A) is the global river Q-A relationship from Syvitski & Milliman (2007). The significance of the difference (slope) test between the gradient from delta Q-A OLS regression versus the global river from Syvitski & Milliman (2007) produces $p = 0.1$.

Figure 5: (A) Climate-classified Q-W relationship from the global deltas; (B-F) Q-W relationships from the arid, cold, polar, temperate and tropical climate regions, respectively. Red continuous lines are the OLS regression obtained from the data shown on each plot. The red dashed line is the regression line obtained from the global river Q-W relationship from Moody & Troutman (2002). Error bars represent median channel width ± 1 standard deviation. The significance of the difference test between the gradient from delta Q-W OLS regression versus the global river equation from Moody & Troutman (2002) produces $p = 2.6 \times 10^{-5}$.

Figure 6: Ferron Sandstone outcrop photographs from Ivie Creek, Utah showing the distribution of distributary channels and associated lobes of Cretaceous delta deposited along the western margin of Western Interior Seaway. Interpreted distributary channel bodies and paleocurrent directions are redrawn from Braathen et al. (2018).

Figure 7: Comparison of bankfull discharges estimated from previous studies with the estimated bankfull discharges calculated using the *Q*-*W* and *Q*-*A* relationships, both global and climate-specific, proposed in this study (Sageman & Arthur, 1994; Bhattacharya & MacEachern, 2009; Bhattacharya *et al.*, 2016).

TABLE CAPTIONS

Table 1: Secondary delta channel width data from the literature and predicted *Q* values from both *Q*-*A* and *Q*-*W* relationships.

Table 2: Summary of the scaling relationships proposed in this study.

Figure 1

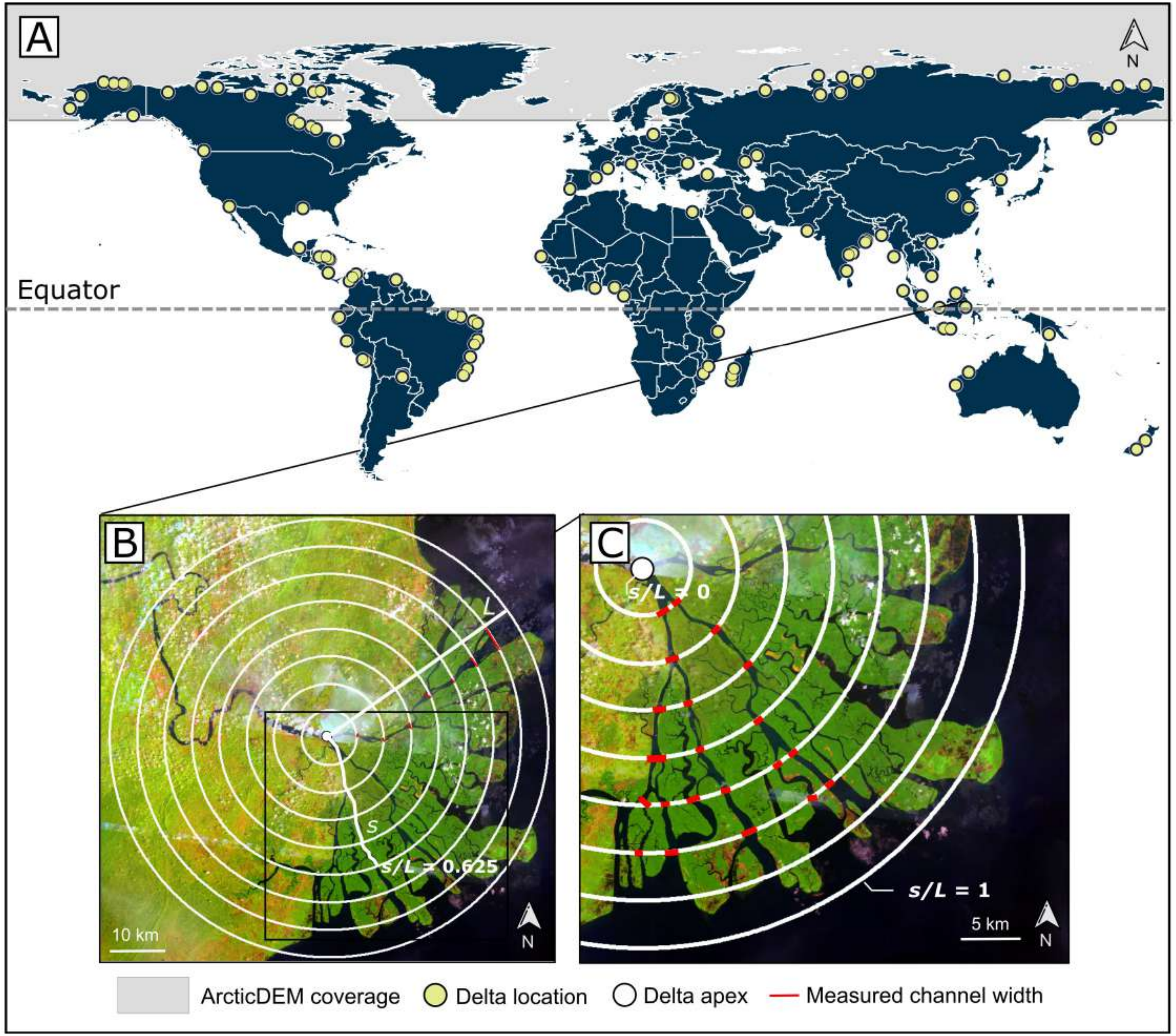

A
N
Equator
B
L
S
s/L = 0.625
10 km
N
C
s/L = 0
s/L = 1
5 km
N
ArcticDEM coverage
Delta location
Delta apex
Measured channel width

Figure 2

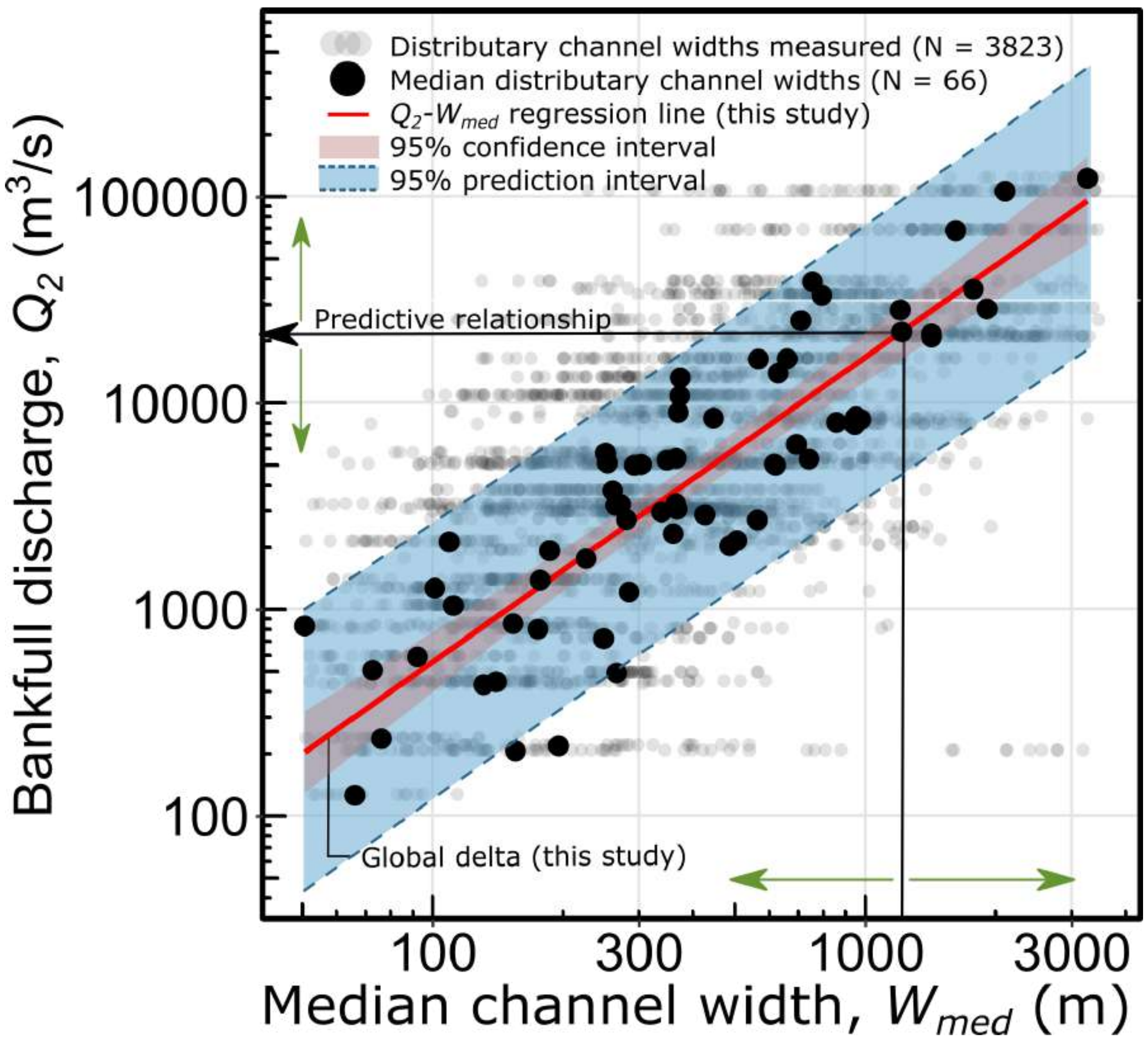

Distributary channel widths measured (N = 3823)
Median distributary channel widths (N = 66)
Q_2-W_{med} regression line (this study)
95% confidence interval
95% prediction interval
Predictive relationship
Global delta (this study)
Bankfull discharge, Q_2 (m^3/s)
100000
10000
1000
100
100
300
1000
3000
Median channel width, W_{med} (m)

Figure 3

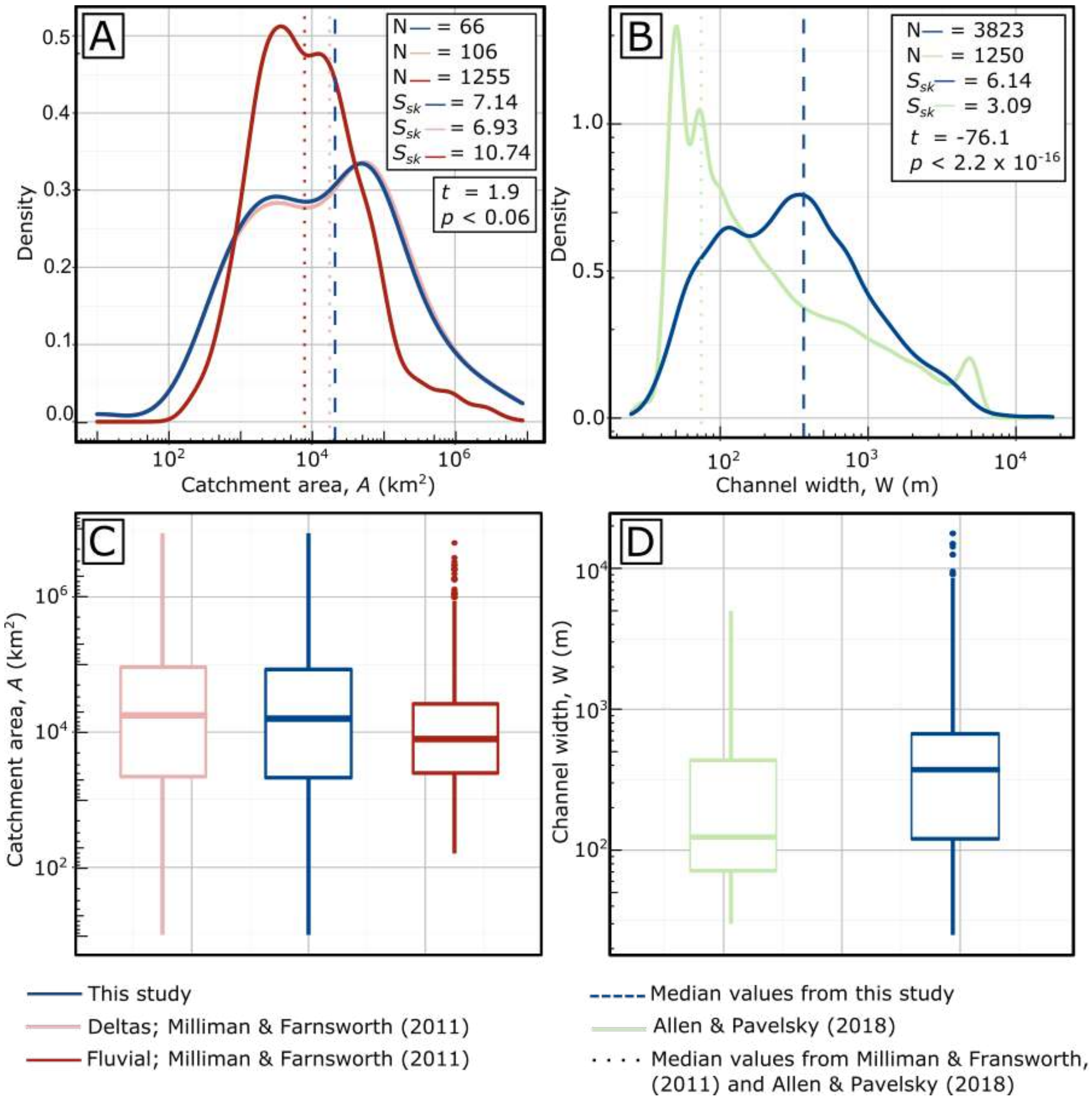

A
N — = 66
N — = 106
N — = 1255
S_{sk} — = 7.14
S_{sk} — = 6.93
S_{sk} — = 10.74
t = 1.9
p < 0.06
Density
Catchment area, A (km^2)
B
N — = 3823
N — = 1250
S_{sk} — = 6.14
S_{sk} — = 3.09
t = -76.1
$p < 2.2 \times 10^{-16}$
Density
Channel width, W (m)
C
Catchment area, A (km^2)
D
Channel width, W (m)
This study
Deltas; Milliman & Farnsworth (2011)
Fluvial; Milliman & Farnsworth (2011)
Median values from this study
Allen & Pavelsky (2018)
Median values from Milliman & Fransworth, (2011) and Allen & Pavelsky (2018)

Figure 4

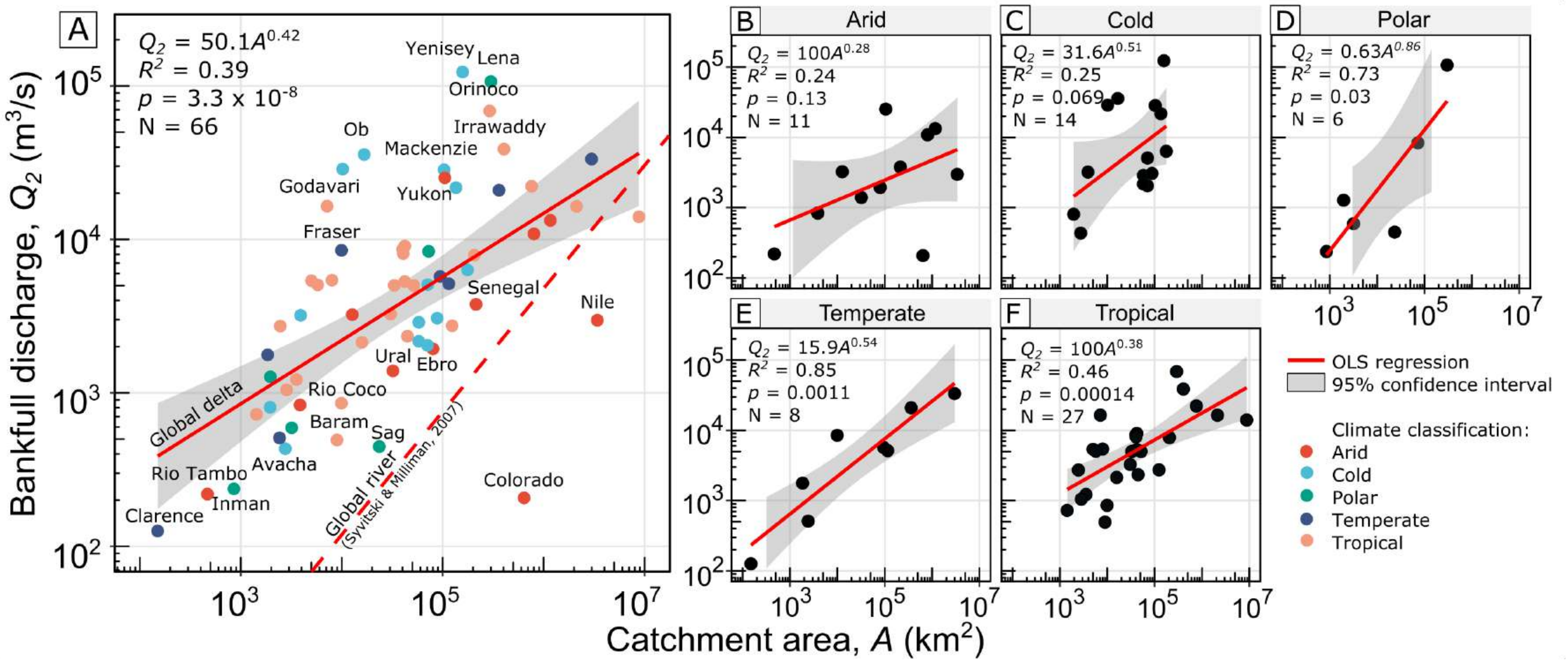

A
$Q_2 = 50.1A^{0.42}$
$R^2 = 0.39$
$p = 3.3 \times 10^{-8}$
N = 66
Bankfull discharge, Q_2 (m^3/s)
Yenisey
Lena
Orinoco
Irrawaddy
Ob
Mackenzie
Godavari
Yukon
Fraser
Senegal
Nile
Ural
Ebro
Rio Coco
Baram
Sag
Avacha
Rio Tambo
Inman
Clarence
Colorado
Global delta
Global river (Syvitski & Milliman, 2007)
B Arid
$Q_2 = 100A^{0.28}$
$R^2 = 0.24$
$p = 0.13$
N = 11
C Cold
$Q_2 = 31.6A^{0.51}$
$R^2 = 0.25$
$p = 0.069$
N = 14
D Polar
$Q_2 = 0.63A^{0.86}$
$R^2 = 0.73$
$p = 0.03$
N = 6
E Temperate
$Q_2 = 15.9A^{0.54}$
$R^2 = 0.85$
$p = 0.0011$
N = 8
F Tropical
$Q_2 = 100A^{0.38}$
$R^2 = 0.46$
$p = 0.00014$
N = 27
Catchment area, A (km^2)
OLS regression
95% confidence interval
Climate classification:
Arid
Cold
Polar
Temperate
Tropical

Figure 5

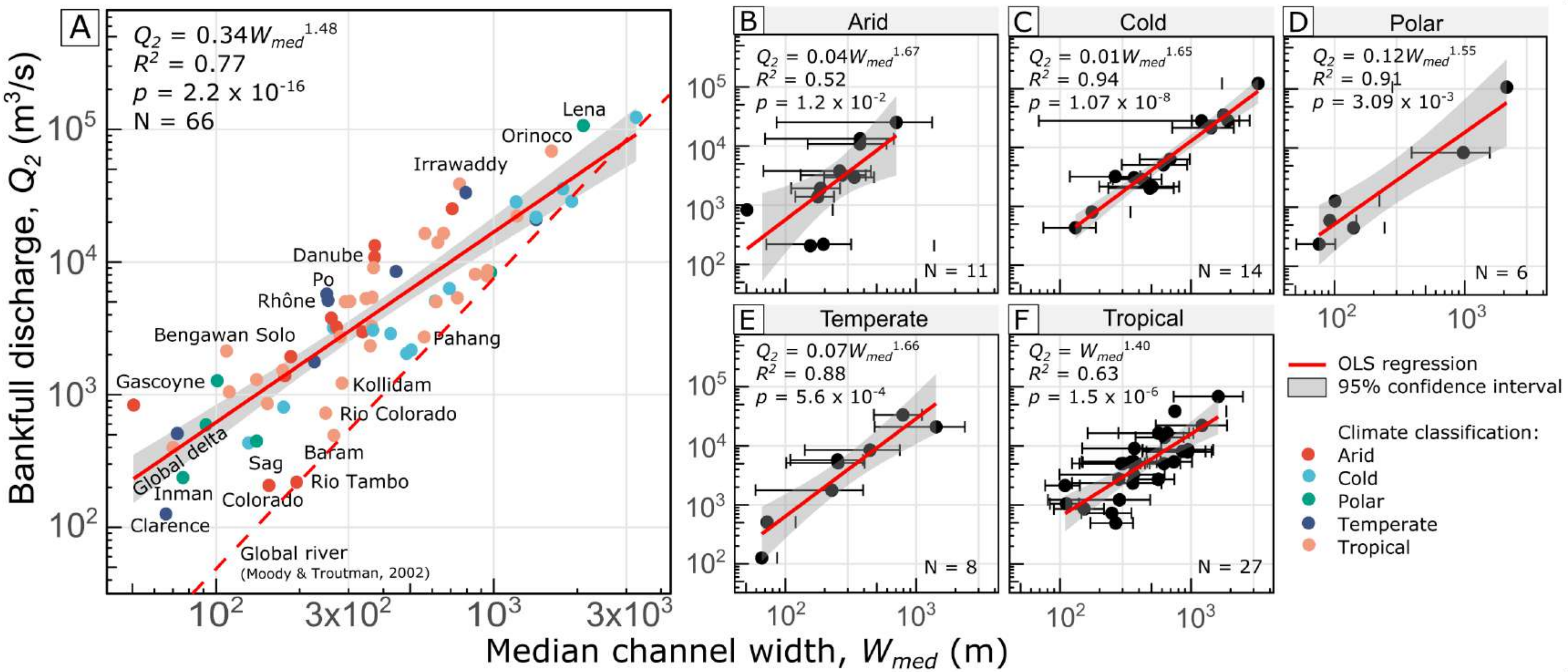

A
$Q_2 = 0.34W_{med}^{1.48}$
$R^2 = 0.77$
$p = 2.2 \times 10^{-16}$
N = 66
Bankfull discharge, Q_2 (m^3/s)
Lena
Orinoco
Irrawaddy
Danube
Po
Rhône
Bengawan Solo
Pahang
Gascoyne
Kollidam
Rio Colorado
Global delta
Baram
Sag
Rio Tambo
Inman
Colorado
Clarence
Global river
(Moody & Troutman, 2002)
B Arid
$Q_2 = 0.04W_{med}^{1.67}$
$R^2 = 0.52$
$p = 1.2 \times 10^{-2}$
N = 11
C Cold
$Q_2 = 0.01W_{med}^{1.65}$
$R^2 = 0.94$
$p = 1.07 \times 10^{-8}$
N = 14
D Polar
$Q_2 = 0.12W_{med}^{1.55}$
$R^2 = 0.91$
$p = 3.09 \times 10^{-3}$
N = 6
E Temperate
$Q_2 = 0.07W_{med}^{1.66}$
$R^2 = 0.88$
$p = 5.6 \times 10^{-4}$
N = 8
F Tropical
$Q_2 = W_{med}^{1.40}$
$R^2 = 0.63$
$p = 1.5 \times 10^{-6}$
N = 27
OLS regression
95% confidence interval
Climate classification:
Arid
Cold
Polar
Temperate
Tropical
Median channel width, W_{med} (m)

Figure 6

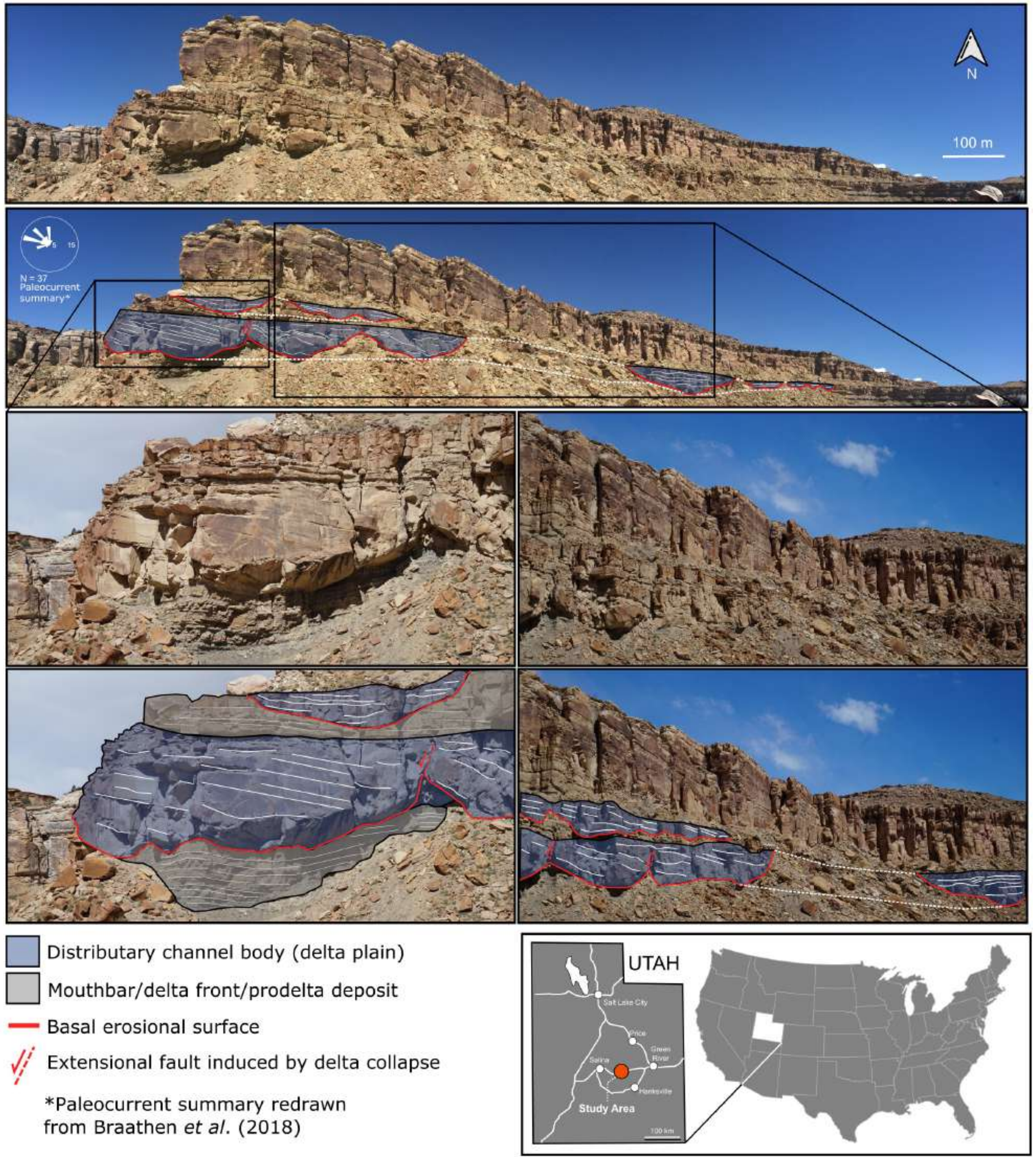
N
100 m
N = 37
Paleocurrent
summary*
Distributary channel body (delta plain)
Mouthbar/delta front/prodelta deposit
Basal erosional surface
Extensional fault induced by delta collapse
*Paleocurrent summary redrawn
from Braathen *et al.* (2018)
UTAH
Salt Lake City
Price
Green River
Salina
Hanksville
Study Area
100 km

Figure 7

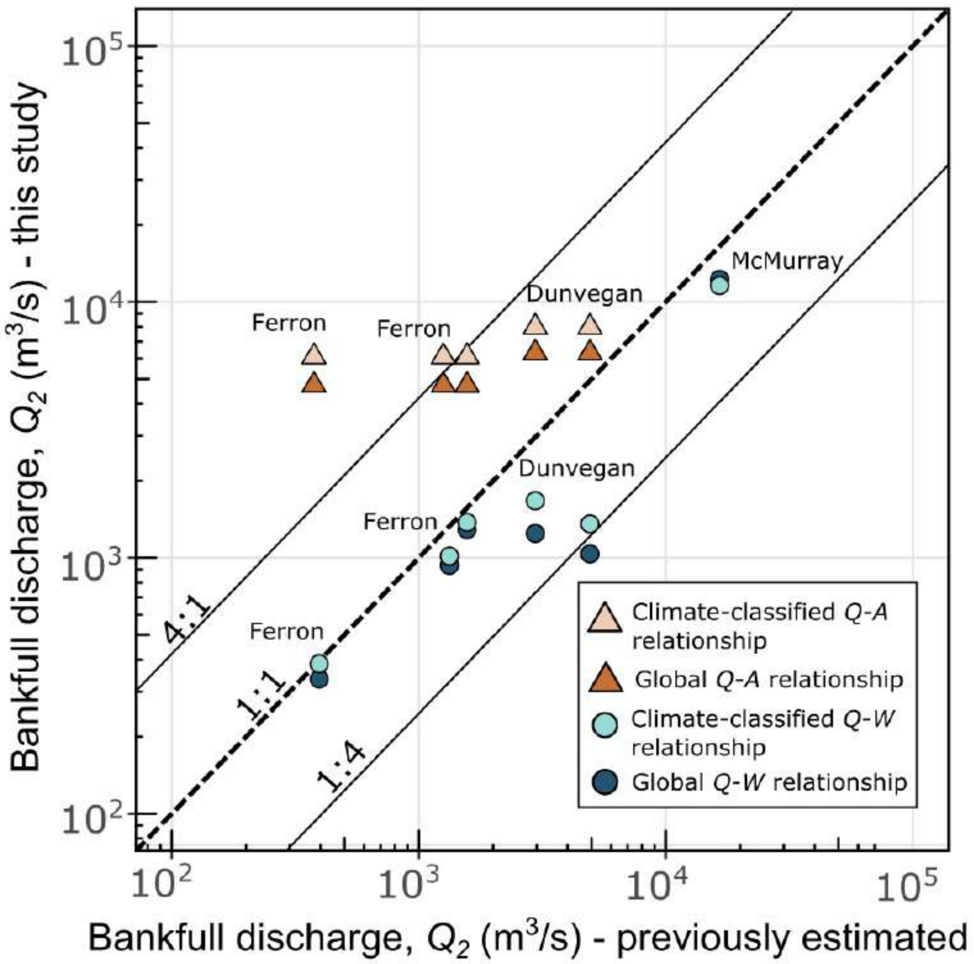

Ferron
Ferron
Dunvegan
McMurray
Dunvegan
Ferron
Ferron
4:1
1:1
1:4
Climate-classified Q-A relationship
Global Q-A relationship
Climate-classified Q-W relationship
Global Q-W relationship
Bankfull discharge, Q2 (m3/s) - this study
Bankfull discharge, Q2 (m3/s) - previously estimated

Table 1

Formation Name	Channel Width (m)	Estimated Paleodischarge (m^3/s)	Paleodrainage area (km^2)	Geological age	Predicted *Q* from global *Q-A* relationship (m^3/s)	Predicted *Q* from climate-classified *Q-A* relationship (m^3/s)	Predicted *Q* from global *Q-W* relationship (m^3/s)	Predicted *Q* from climate-classified *Q-W* relationship (m^3/s)	Source
Ferron[1]	174	1525	50000	Turonian	6104 ± 87900	4714 ± 87900	1284 ± 527	1370 ± 527	Sageman & Arthur, 1994; Bhattacharya & MacEachern, 2009
Ferron[2]	140	1300	50000	Turonian	6104 ± 87900	4714 ± 87900	930 ± 527	1011 ± 527	Bhattacharya *et al.*, 2016
Ferron[3]	70	400	50000	Turonian	6104 ± 87900	4714 ± 87900	334 ± 527	383 ± 527	Bhattacharya *et al.*, 2016
Dunvegan	170	2829	100000	Cenomanian	7969 ± 87900	6307 ± 87900	1240 ± 527	1664 ± 527	Sageman & Arthur, 1994; Bhattacharya & MacEachern, 2009
Dunvegan[2]	150	4641	100000	Cenomanian	7969 ± 87900	6307 ± 87900	1030 ± 527	1352 ± 527	Sageman & Arthur, 1994; Bhattacharya & MacEachern, 2009
McMurray	800	15000	NA	Barremian-Aptian	NA	NA	12273 ± 527	11597 ± 527	Bhattacharya *et al.*, 2016

[1,2,3]end members channel width measurement extracted from the literature

± represents 95% prediction intervals from the global dataset. Wide prediction intervals are due to scatter in the data and the small number of deltas measured in this study, leading to high standard error of the residuals.

Table 2

Water discharge and catchment area scaling relationships			
Classification	N	Equation	Statistical significance
Global	66	$Q_2 = 50.1A^{0.42}$	$R^2 = 0.39$; $p = 3.3 \times 10^{-8}$
Arid	11	$Q_2 = 100A^{0.28}$	$R^2 = 0.24$; $p = 1.3 \times 10^{-1}$
Cold	14	$Q_2 = 31.6A^{0.51}$	$R^2 = 0.25$; $p = 6.9 \times 10^{-2}$
Polar	6	$Q_2 = 0.63A^{0.86}$	$R^2 = 0.73$; $p = 3 \times 10^{-2}$
Temperate	8	$Q_2 = 15.9A^{0.54}$	$R^2 = 0.85$; $p = 1.1 \times 10^{-3}$
Tropical	27	$Q_2 = 100A^{0.38}$	$R^2 = 0.46$; $p = 1.4 \times 10^{-4}$
Water discharge and median channel width scaling relationships			
Classification	N	Equation	Statistical significance
Global	66	$Q_2 = 0.34W_{med}^{1.48}$	$R^2 = 0.77$; $p = 2.2 \times 10^{-16}$
Arid	11	$Q_2 = 0.04W_{med}^{1.67}$	$R^2 = 0.52$; $p = 1.2 \times 10^{-2}$
Cold	14	$Q_2 = 0.01W_{med}^{1.65}$	$R^2 = 0.94$; $p = 1.07 \times 10^{-8}$
Polar	6	$Q_2 = 0.12W_{med}^{1.55}$	$R^2 = 0.91$; $p = 3.09 \times 10^{-3}$
Temperate	8	$Q_2 = 0.07W_{med}^{1.66}$	$R^2 = 0.88$; $p = 5.6 \times 10^{-4}$
Tropical	27	$Q_2 = W_{med}^{1.4}$	$R^2 = 0.63$; $p = 1.5 \times 10^{-6}$

Supporting information

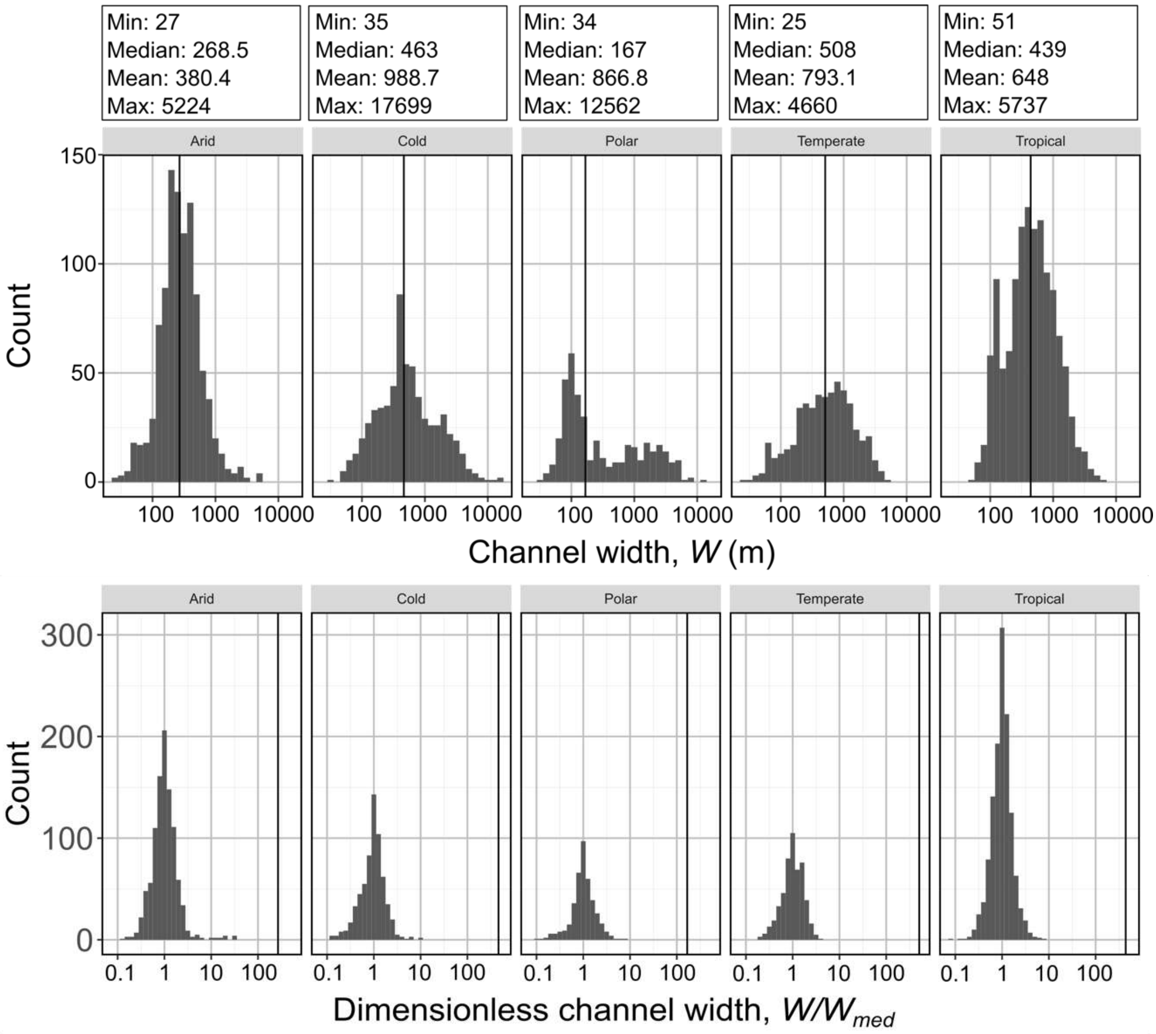

Figure S1: (A) Histograms showing the distribution of measured distributary channel widths and (B) dimensionless channel width (W/W_{med}) from arid, cold, polar, temperate, and tropical climate region, consecutively. Vertical lines on the plots (A) refers to median channel width values for each climate region.

Table S1. In-situ measurement of width and depth of several river deltas collected from the literature.

Location	Year	Width (W) (m)	Depth (d) (m)	W:d ratio (-)	Note	Source
Lijin, Yellow delta	1977	621	6.26	99.14	Depth is defined as the averaged bed level in the deepest part of the channel width from a cross-sectional area of 500 m^2	https://doi.org/10.1016/S1001-6279(08)60002-5
Lijin, Yellow delta	1987	615	6.60	93.19	Depth is defined as the averaged bed level in the deepest part of the channel	https://doi.org/10.1016/S1001-6279(08)60002-5

					width from a cross-sectional area of 500 m^2	
Lijin, Yellow delta	1997	622	5.14	121.01	Depth is defined as the averaged bed level in the deepest part of the channel width from a cross-sectional area of 500 m^2	https://doi.org/10.1016/S1001-6279(08)60002-5
Lijin, Yellow delta	1950-1999			200	*W:d = f(Qw)*, using the same data as above	https://doi.org/10.1016/j.quaint.2010.09.002
35 km above Head of Passes, Mississippi delta	1974-1975	800	22	36	*Qw* > 35.000 m^3/s, depth is calculated by differencing the water-surface elevation from the 40th-percentile depth from the distribution of all wetted elevations for a transect, beginning from the channel bed.	https://doi.org/10.1130/B30497.1
100 km above Head of Passes, Mississippi delta	1974-1975	770	23	33.48	*Qw* > 35.000 m^3/s, depth is calculated by differencing the water-surface elevation from the 40th-percentile depth from the distribution of all wetted elevations for a transect, beginning from the channel bed.	https://doi.org/10.1130/B30497.1
200 km above Head of Passes, Mississippi delta	1974-1975	750	20	37.5	*Qw* > 35.000 m^3/s, depth is calculated by differencing the water-surface elevation from the 40^{th}-percentile depth from the distribution of all wetted elevations for a transect, beginning from the channel bed.	https://doi.org/10.1130/B30497.1
Fly				15-30	Meandering, slope is always very gentle	http://dx.doi.org/10.1016/j.geomorph.2008.05.035
Amazon				20 - >100	Anabranching, suspended load dominant	http://dx.doi.org/10.1016/j.geomorph.2008.05.035
Brahmaputra				>100	Complex anabranching	http://dx.doi.org/10.1016/j.geomorph.2008.05.035
Atchafalaya Delta	1983			Few hundreds	Depth is measured from the terminal distributary channel	doi: 10.2110/jsr.2006.026

Wax Lake Delta	2002			Few hundreds	Depth is measured from the terminal distributary channel	doi: 10.2110/jsr.2006.026
Volga Delta	2000	10-20	1-3	±10	Depth is measured from the terminal distributary channel	doi: 10.2110/jsr.2006.026
Lena Delta	2000	100-400	1	100-400	Width is taken from the highest frequency from their Fig. 8E	doi: 10.2110/jsr.2006.026
Eocene Battfjellet Deltas		50-200	5	10-40	-	doi: 10.2110/jsr.2006.026
Kapuas Delta	2013-2015			16-128	-	doi:10.1002/2016JF004075

Table S2. Global and climate-classified discharge:depth (*Q-d*) scaling relationships proposed based on three width:depth (*W:d*) ratios found from a number of modern river deltas.

Classification	$W:d$ = 30:1	$W:d$ = 100:1	$W:d$ = 200:1
Global	$Q = 54.95d^{1.69}$ $R^2 = 0.76$ $P < 2.2 \times 10^{-17}$	$Q = 421.7d^{1.69}$ $R^2 = 0.77$ $P < 2.2 \times 10^{-17}$	$Q = 1349d^{1.69}$ $R^2 = 0.77$ $P < 2.2 \times 10^{-17}$
Arid	$Q = 19.95d^{2.32}$ $R^2 = 0.52$ $P = 1.2 \times 10^{-2}$	$Q = 331.13d^{2.32}$ $R^2 = 0.52$ $P = 1.2 \times 10^{-2}$	$Q = 1659.59d^{2.32}$ $R^2 = 0.52$ $P = 1.2 \times 10^{-2}$
Cold	$Q = 33.11d^{1.70}$ $R^2 = 0.94$ $P = 1.1 \times 10^{-8}$	$Q = 263.02d^{1.70}$ $R^2 = 0.94$ $P = 1.1 \times 10^{-8}$	$Q = 794.33d^{1.70}$ $R^2 = 0.94$ $P = 1.1 \times 10^{-8}$
Polar	$Q = 67.6d^{1.63}$ $R^2 = 0.91$ $P = 3.1 \times 10^{-3}$	$Q = 481.95d^{1.63}$ $R^2 = 0.91$ $P = 3.1 \times 10^{-3}$	$Q = 1479.11d^{1.63}$ $R^2 = 0.91$ $P = 3.1 \times 10^{-3}$
Temperate	$Q = 68.11d^{1.77}$ $R^2 = 0.88$ $P = 5.6 \times 10^{-4}$	$Q = 571.08d^{1.77}$ $R^2 = 0.88$ $P = 5.6 \times 10^{-4}$	$Q = 1940.89d^{1.77}$ $R^2 = 0.88$ $P = 5.6 \times 10^{-4}$
Tropical	$Q = 43.65d^{1.77}$ $R^2 = 0.63$ $P = 1.5 \times 10^{-6}$	$Q = 371.54d^{1.77}$ $R^2 = 0.63$ $P = 1.5 \times 10^{-6}$	$Q = 1255.59d^{1.77}$ $R^2 = 0.63$ $P = 1.5 \times 10^{-6}$